JOC The Journal of Organic Chemistry

pubs.acs.org/joc Article

Linear Extension of Carbaporphyrin Chromophores: Synthesis, Protonation, and Metalation of Anthro[2,3-*b*]carbaporphyrins: Evidence for 30π-Electron Aromatic Circuits in a Palladium(II) Complex

Melissa A. Mathius, Justin M. Chhoeun, Riley H. Kaufman, Deyaa I. AbuSalim, and Timothy D. Lash*

Cite This: https://doi.org/10.1021/acs.joc.3c01839 Read Online

ACCESS | Metrics & More | Article Recommendations | Supporting Information

ABSTRACT: Acid-catalyzed condensation of a naphtho[2,3-*f*]indane dialdehyde with a tripyrrane, followed by an oxidation step, afforded an anthro[2,3-*b*]-21-carbaporphyrin. The presence of a fused anthracene unit induced minor bathochromic shifts and did not significantly affect the aromatic characteristics of the carbaporphyrin core. Protonation led to the formation of a monocation with similar diatropic properties, but the dication generated in the presence of a large excess of trifluoroacetic acid had a weakened Soret band absorption and a broad absorption at 754 nm. Nucleus-independent chemical shift (NICS) calculations indicate that the dication is only weakly aromatic and possesses a 32-atom 30π electron delocalization pathway. Alkylation with methyl iodide and potassium carbonate gave a 22-methyl derivative that reacted with palladium(II) acetate to afford an aromatic palladium(II) complex. Upon heating, the methyl group migrated from the nitrogen to the internal carbon atom and the resulting complex exhibited diminished aromatic character. A comparison with related carbaporphyrin complexes without ring fusion or with benzo- or naphtho-fused units demonstrated that the diatropic character decreased with increasing conjugation. NICS calculations and anisotropy of induced current density (AICD) plots confirmed this trend and showed that the remaining aromatic properties of the anthrocarbaporphyrin complex were due to a 30π electron circuit that extends around the entire anthracene unit.

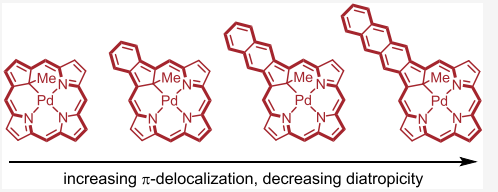

INTRODUCTION

Carbaporphyrinoid systems exhibit diverse spectroscopic characteristics and intriguing reactivity.[1] True carbaporphyrins, which possess cyclopentadiene units or related annulated derivatives such as indene in place of the usual pyrrolic moieties within the porphyrin framework, have fully aromatic properties and give electronic absorption spectra that closely resemble regular porphyrins. Carbaporphyrins have unique reactivity and readily form organometallic derivatives with late transition metal cations.[2,3] Much of the work in this area has been conducted on benzo-fused carbaporphyrins **1** (Scheme 1) due in part to ease of synthesis.[4] In principle, ring fusion extends conjugation within these porphyrinoid systems, but in practice, **1** still favors an 18π electron delocalization pathway. Benzocarbaporphyrins afford organometallic derivatives with Ag (e.g., **2**),[5] Au,[5] Ir,[6] Rh,[6] and Re.[7] Alternatively, reaction of **1** with ferric chloride in the presence of alcohol solvents selectively oxidized the carbaporphyrin core to give carbaporphyrin ketals **3**.[8] Not only do these derivatives possess modified chromophores with relocated aromatic delocalization pathways, they also show promise in the treatment of leishmaniasis.[9] Carbaporphyrins readily protonate to give monocations $\mathbf{1}H^+$ and in the presence of a large excess of trifluoroacetic acid generate C-protonated dications $\mathbf{1}H_2^{2+}$. The latter species again relocates the conjugation pathway around the carbocyclic ring. Furthermore, *N*-alkyl carbaporphyrins **4** react with palladium(II) acetate to initially afford palladium complexes **5**, but these undergo an irreversible rearrangement to give C-alkyl complexes **6**.[10,11] These derivatives also possess highly modified chromophores and introduce a continuous 22π electron circuit in conjunction with the fused benzene ring.

Polycyclic graphene and heterographene structures such as annulated porphyrins have received considerable attention in recent years.[12−16] In a contribution to this area, we have previously reported the synthesis of a naphthalene-fused carbaporphyrin **7** (Figure 1) to investigate how extended conjugation affects carbaporphyrin structures.[17] In this paper, the effects caused by further extension of the linearly fused unit on the carbaporphyrin system are reported. Specifically, the first examples of anthro[2,3-*b*]carbaporphyrins **8** have been synthesized[18] and the resulting modifications to the carbaporphyrin system due to the fused anthracene unit have been investigated. Although only minor effects were noted for the free

Received: August 14, 2023
Revised: October 31, 2023
Accepted: December 7, 2023

https://doi.org/10.1021/acs.joc.3c01839
J. Org. Chem. XXXX, XXX, XXX−XXX

Scheme 1. Selected Reactions of Benzocarbaporphyrin 1

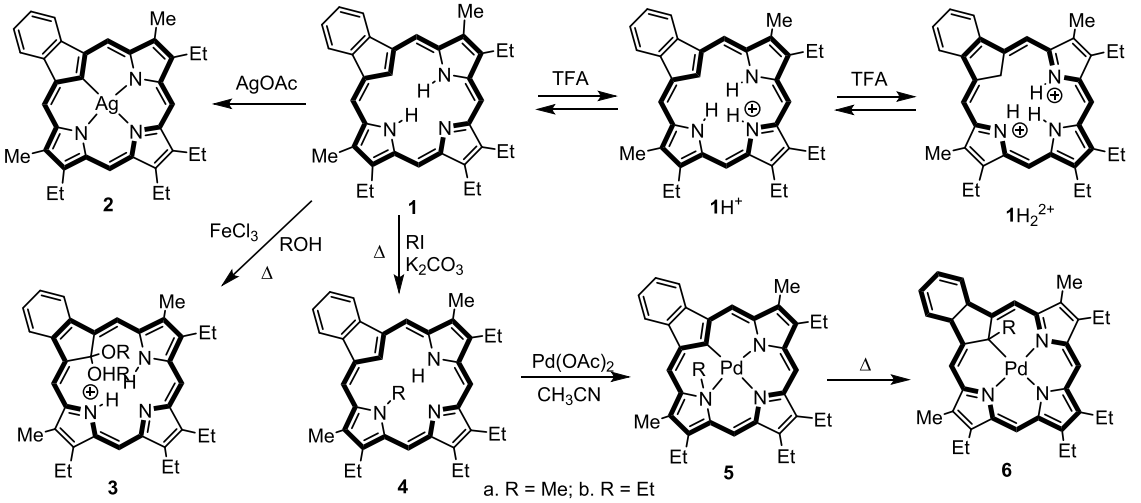

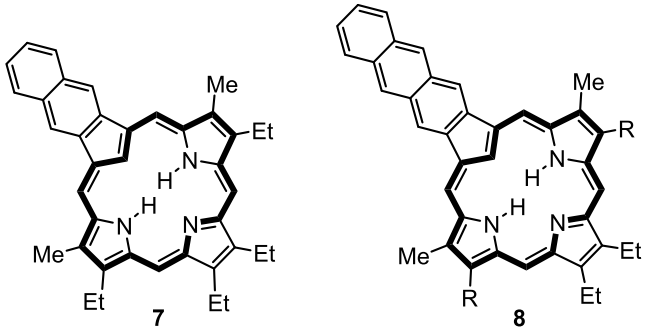

Figure 1. Naphtho- and Anthrocarbaporphyrins.

base porphyrinoids, a related palladium(II) complex showed dramatic changes that implicated the presence of a 30π electron delocalization pathway.

RESULTS AND DISCUSSION

Synthesis and Metalation of Anthrocarbaporphyrins. The key intermediate in the synthesis of anthrocarbaporphyrin **8** was naphtho[2,3-*f*]Indane dialdehyde **9**. Diels–Alder cycloaddition of cyclopentadiene with 1,4-anthroquinone **10** afforded adduct **11**, and this was reduced to the corresponding dialcohol **12** with sodium borohydride (Scheme 2).[19] Reaction with *p*-toluenesulfonyl chloride and pyridine generated anthronorbornadiene **13**, and this reacted with tetra-*n*-butylammonium permanganate in dichloromethane to produce diol **14**. This in turn was reacted with potassium periodate in THF–water to give the required *cis*-dialdehyde **9**. The dialdehyde was reasonably stable and could be stored in the freezer for several months without significant degradation occurring. However, the dialdehyde decomposed if purification was attempted by column chromatography. Although some of the dialdehyde could still be collected, isomerization afforded an approximately 1:1 mixture of *cis* and *trans* isomers.

Anthro[2,3-*b*]-21-carbaporphyrin **8** was prepared using the '3 + 1' modification of the MacDonald condensation (Scheme 3).[20] In previous studies, the presence of fused aromatic rings greatly reduced the solubility of porphyrin-type structures, but the introduction of long alkyl chains can mitigate this problem.[21] With this in mind, dihexyltripyrrane **15**[21] was reacted with dialdehyde **9** in the presence of trifluoroacetic acid (TFA), and

Scheme 2. Synthesis of a Naphthoindane Dialdehyde

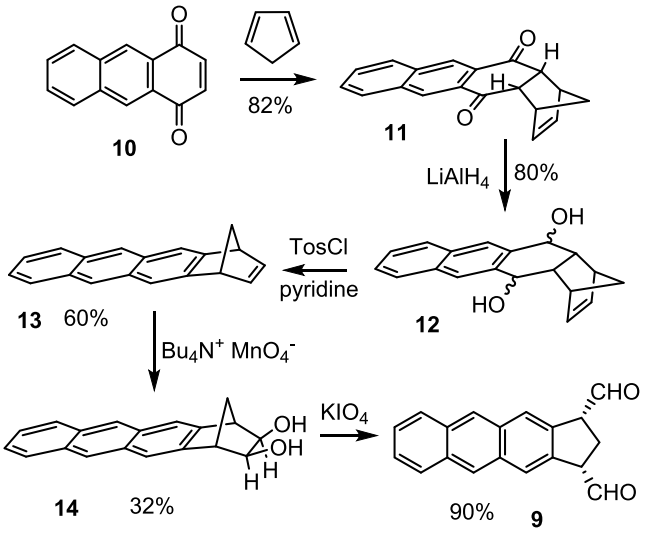

following oxidation with 2,3-dichloro-5,6-dicyano-1,4-benzoquinone (DDQ), anthrocarbaporphyrin **8** was isolated in up to 36% yield (Scheme 3). Anthracene-fused carbaporphyrin **8** proved to be reasonably soluble in chloroform, demonstrating that the presence of two long hydrocarbon chains was sufficient to overcome π-stacking interactions due to the anthracene unit.

The UV–vis spectrum of free base anthrocarbaporphyrin **8** in chloroform gave a split Soret band at 426 and 448 nm along with a series of Q bands at 530, 569, 615, and 677 nm (Figure 2). This contrasts with naphthocarbaporphyrin **7**[17] which showed a Soret band at 432 nm and Q bands at 517, 554, 607, and 668 nm. Hence, the fusion of an additional benzene ring induces significant bathochromic shifts indicating that there are at least some minor interactions between the core carbaporphyrin chromophore and the anthracene unit. Upon spectroscopic titration with TFA, anthrocarbaporphyrin **8** exhibited significant bathochromic shifts that can be attributed to the formation of monoprotonated species $\mathbf{8}H^+$ (Figure 3 and Scheme 3). The resulting electronic absorption spectra gave rise to three strongly shifted Soret bands at 418, 449, and 478 nm. At much higher concentrations of TFA, a diprotonated species $\mathbf{8}H_2^{2+}$ was observed. In 50% trifluoroacetic acid, this species gave a weak

https://doi.org/10.1021/acs.joc.3c01839
J. Org. Chem. XXXX, XXX, XXX–XXX

Scheme 3. Synthesis and Protonation of an Anthrocarbaporphyrin

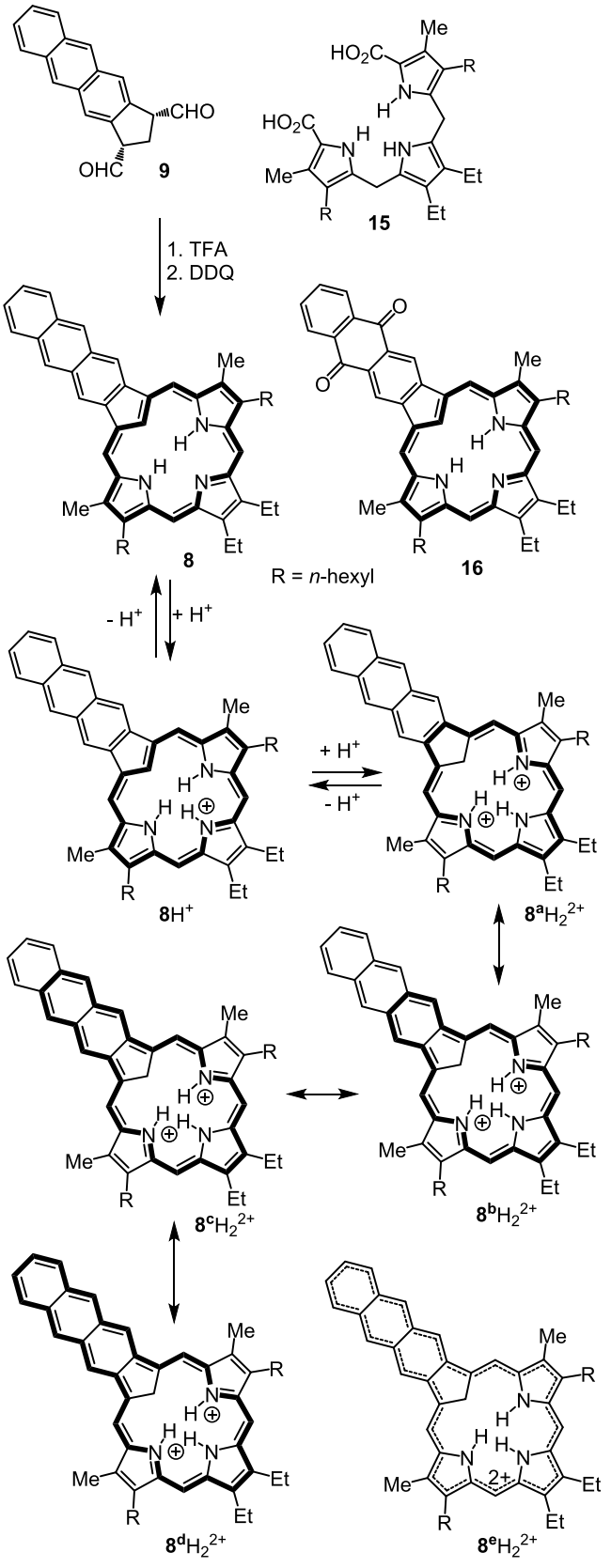

Soret band at 399 nm along with Q bands at 506 and 755 nm (Figure 3). This species has a considerably different electronic absorption spectrum compared to the free base and monoprotonated forms. Furthermore, dications derived from benzocarbaporphyrin or naphthocarbaporphyrin still have strong Soret-like bands at 436 and 455 nm, respectively, but also show relatively strong absorptions in the red or far-red region (Table 1). In dication $\mathbf{8}H_2^{2+}$, the anthracene unit more effectively extends the π-system and can potentially introduce the 18, 22, 26, and 30π electron circuits shown in bold for resonance structures $\mathbf{8}^{a}H_2^{2+}$, $\mathbf{8}^{b}H_2^{2+}$, $\mathbf{8}^{c}H_2^{2+}$, and $\mathbf{8}^{d}H_2^{2+}$ (Scheme 3). Alternatively, this species can be envisaged as a bridged [32]annulene dication as illustrated in structure $\mathbf{8}^{e}H_2^{2+}$ (Scheme 3). It appears that these extended conjugation pathways undermine the porphyrin-like character of the system. Unfortunately, attempts to obtain a proton NMR spectrum for dication $\mathbf{8}H_2^{2+}$ were not successful.

The proton NMR spectrum for free base anthro[2,3-*b*]carbaporphyrin **8** in $CDCl_3$ demonstrated that the system retains strongly diatropic characteristics (Figure 4). The external *meso*-protons gave two 2H downfield singlets at 9.80 and 9.69 ppm, while the inner CH resonance appeared upfield at −6.54 ppm. Additionally, the anthracene protons gave rise to two 2H singlets at 9.05 (2^1,3^1-H) and 8.72 (2^2,3^2-H) ppm and two 2H multiplets at 8.15 (2^3,3^3-H) and 7.55 (2^4,3^4-H) ppm. While the 2^1,3^1-protons are shifted downfield due to their spatial proximity to the macrocyclic ring current, the remaining values are typical of substituted anthracenes, suggesting that the porphyrinoid ring current does not pass through this fused aromatic unit. This phenomenon is also seen in naphthocarbaporphyrin **7** as the naphthalene protons appear as a 2H singlet at 9.06 ppm and two 2H multiplets at 8.26 and 7.63 ppm.[17] Additionally, the *meso*-protons of **7** appear further downfield at 10.00 and 9.76 ppm, while the inner CH shows up at −6.55 ppm,[17] suggesting that the addition of the third fused ring slightly decreases the diamagnetic ring current in **8**. Benzocarbaporphyrin **1** follows this trend as the *meso*-protons appear even further downfield at 10.10 and 9.82 ppm, while the internal CH resonates further upfield at −6.74 ppm.[4] The carbon-13 NMR spectrum for **8** in $CDCl_3$ confirmed that the macrocycle has a plane of symmetry, and the *meso*-carbons gave rise to two peaks at 96.2 and 96.3 ppm, while the internal CH appeared at 114.6 ppm.

In addition to giving the targeted anthrocarbaporphyrin, reaction of dialdehyde **9** with tripyrrane **15** gave rise to minor byproducts most of which could not be identified. However, a minor green, slightly more polar, fraction was observed that showed porphyrin-like characteristics and the UV−vis spectrum for this species gave a strong Soret band at 407 nm and several weaker absorptions between 450 and 650 nm. High-resolution TOF-ESI MS gave an [M + H] peak at 742.4383 that corresponds to a species with the molecular formula $C_{51}H_{55}N_3O_2$. Although the byproduct has poor solubility in organic solvents, NMR data could be collected in $CDCl_3$ at 55 °C. The proton NMR spectrum showed that the system has a plane of symmetry, and the *meso*-protons were identified as two 2H singlets at 9.85 and 9.67 ppm. Resonances for 2 equiv methyl, ethyl, and hexyl substituents were evident. Additionally, a 2H singlet at 9.37 ppm and two 2H multiplets at 8.50 and 7.85 ppm were present in the downfield region, demonstrating that two of the anthracene protons were missing, and these data are consistent with the formation of a fused anthraquinone unit. NOE difference proton NMR spectroscopy showed a correlation between the anthracene resonance at 9.37 ppm and the *meso*-proton resonance at 9.85 ppm, and this observation was sufficient to identify the byproduct as structure **16** (Scheme 3). The carbon-13 NMR spectrum for **16** showed

https://doi.org/10.1021/acs.joc.3c01839
J. Org. Chem. XXXX, XXX, XXX−XXX

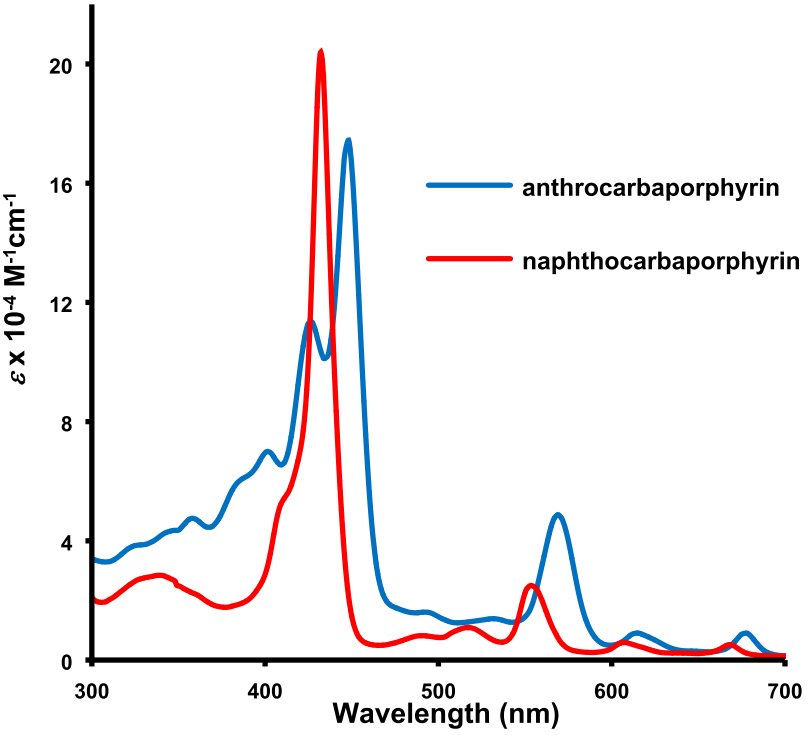

Figure 2. UV−vis spectra of naphthocarbaporphyrin **7**[17] in 1% Et_3N−$CHCl_3$ and anthrocarbaporphyrin **8** in $CHCl_3$.

the *meso*-carbons at 106.4 and 95.2 ppm, and a resonance for the carbonyl moieties was present at 184.1 ppm. Although **16** was only isolated in <1% yield, its formation indicates that the anthracene unit in **8** is prone to oxidation.

The NNNN core of porphyrins has proven to be one of the most versatile platforms for coordination chemistry.[22] Altering the macrocyclic core to CNNN decreases reactivity toward metal cations, but carbaporphyrinoid systems still form stable organometallic derivatives.[2,3]

Benzocarbaporphyrins behave as trianionic ligands and it has previously been reported that benzo-[5] and naphthocarbaporphyrins[17] generate silver(III) complexes when reacted with silver(I) acetate at room temperature. In order to investigate the coordination chemistry of the anthrocarbaporphyrin system, **8** was reacted with silver(I) acetate in an attempt to prepare **17** (Scheme 4). Unfortunately, the resulting product was highly insoluble and could not be characterized. In addition, poor-quality proton NMR spectra indicated that the isolated product was impure, possibly due to the anthracene unit being prone to oxidation. Carbaporphyrins have also been shown to form rhodium(I) and rhodium(III) complexes.[6] Anthrocarbaporphyrin **8** was refluxed with 1 equiv of di-μ-chlorotetracarbonyldirhodium(I) in dichloromethane for 16 h and this afforded rhodium(I) complex **18** in 37% yield (Scheme 4). The proton NMR spectrum confirmed that the macrocycle retains strongly diatropic characteristics (Figure 5) and also showed that the system is no longer symmetrical. The loss of symmetry is also evident in the carbon-13 NMR spectrum of **18**, and four resonances for the *meso*-carbons could be identified (Figure 5). The carbonyl ligands afforded two downfield doublets at 178.6 and 177.8 ppm due to coupling with ^{107}Rh (I = 1/2). The proton NMR spectrum of **18** also showed the internal CH resonance at −4.92 ppm, while the NH afforded an upfield peak at −2.32 ppm. The *meso*-proton resonances were observed downfield between 9.75 and 10.30 ppm, indicating that the introduction of rhodium(I) strengthens the ring current. The UV−vis spectrum of **17** gave a Soret-like band 493 nm and several smaller absorptions between 550 and 700 nm (Figure 6). Rhodium(I) complexes of benzo- and naphthocarbaporphyrins were converted into rhodium(III) complexes when heated in pyridine.[6,23] However, when **18** was refluxed in pyridine, the expected rhodium(III) complex **19** did not form and demetalation of the complex to give the original anthrocarbaporphyrin was observed instead. It is not clear why the reaction failed in this case, but it is noteworthy that the rhodium(I) derivative of naphthocarbaporphyrin **7** gave a significantly poorer yield (21%)[23] of the corresponding rhodium(III) complex than was the case for rhodium(I) benzocarbaporphyrin where the rhodium(III) complex was isolated in 90% yield.[6]

Anthrocarbaporphyrin **8** was reacted with methyl iodide and potassium carbonate in refluxing acetone to give asymmetrical *N*-methyl derivative **20** in 49% yield (Scheme 5). No other alkylation products could be identified. The UV−vis spectrum for **20** is slightly red-shifted, most likely due to distortion of the macrocycle from steric crowding within the central cavity. Trace amounts of TFA (1 equiv or less) led to dramatic changes in the absorption spectra due to the formation of a monoprotonated species and this shows that **20** is significantly more basic than **8**. The proton NMR spectrum of **20** demonstrated that the structure is strongly diatropic and the internal CH and methyl resonances were observed at −2.27 and −3.99 ppm, respectively. The *meso*-protons gave rise to four 1H singlets at 10.03, 9.93, 9.66, and 9.51 ppm due to loss of symmetry in the *N*-methyl derivative. It is worth noting that the internal *N*-methyl substituent is too large to pass through the macrocyclic center, making this system chiral and causing it to exist in two enantiomeric forms.

Reaction of **20** with palladium(II) acetate in chloroform-acetonitrile initially gave palladium(II) complex **21**. However,

https://doi.org/10.1021/acs.joc.3c01839
J. Org. Chem. XXXX, XXX, XXX−XXX

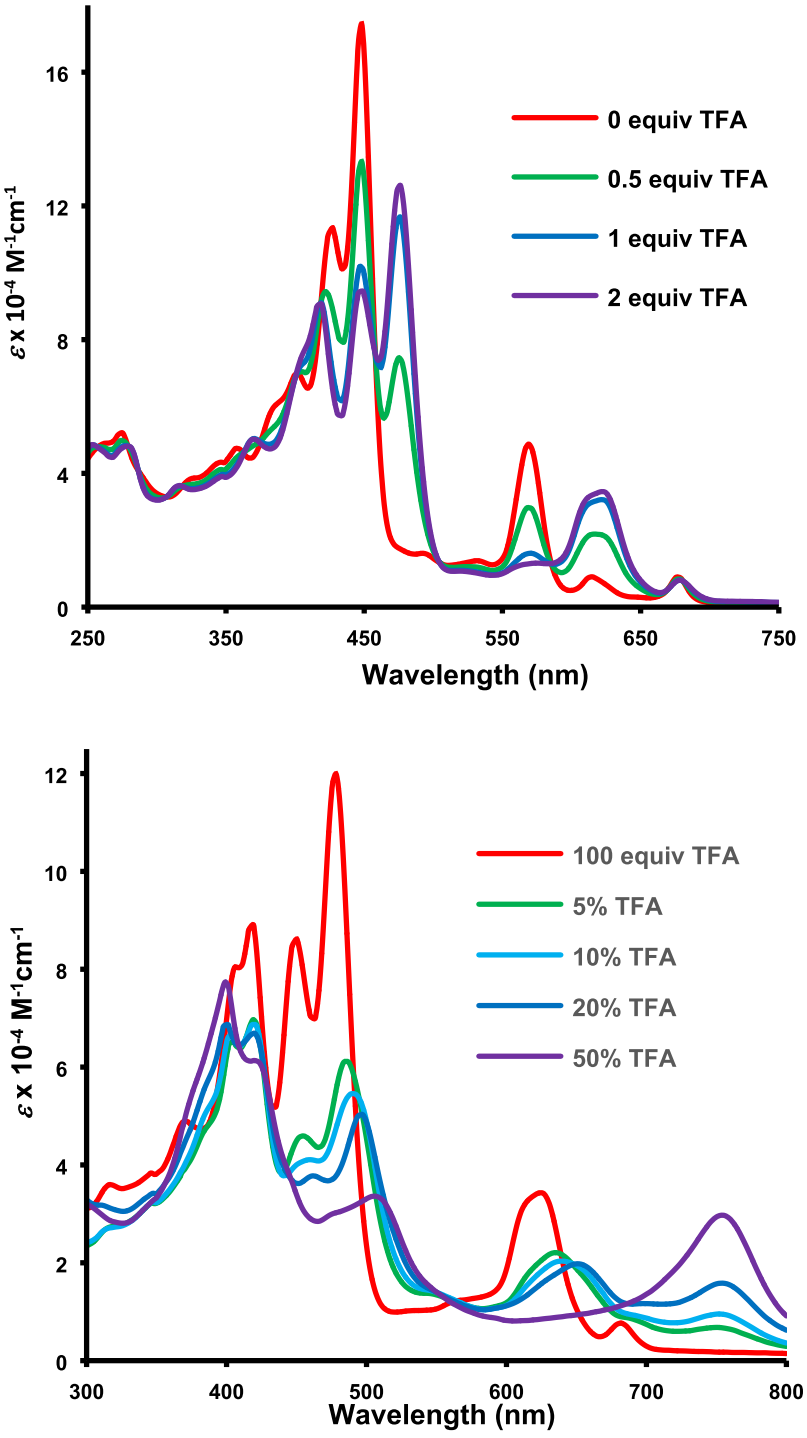

Figure 3. UV−vis spectra of anthrocarbaporphyrin **103** with increasing concentrations of trifluoroacetic acid.

Table 1. UV−vis Spectra (λ_{max}/nm) for Benzo-, Naphtho-, and Anthrocarbaporphyrin Dications[a]

	Soret band	Q bands	
$2H_2^{2+}$	426	614	662
$7H_2^{2+}$	455	708	774
$8H_2^{2+}$	399	506	754

[a]The UV−vis spectra for $2H_2^{2+}$ and $8H_2^{2+}$ were recorded in 50% TFA,[4] while the spectrum for $7H_2^{2+}$ was obtained in 50% TFA-$CHCl_3$.[17].

when the reaction mixture was heated under reflux, methyl group migration was observed to give C-methyl complex **22**. This type of rearrangement has been observed for other carbaporphyrins but in the case of benzocarbaporphyrins **4**, the initial *N*-alkyl products **5** rearranged comparatively rapidly to C-alkyl derivative **6**, and it was not possible to isolate pure **5** (Scheme 1).[10,24] *N*-Methyl complex **20** was generated at room temperature in <10 min and could easily be purified and spectroscopically characterized. A sample of the *N*-methyl intermediate was placed in an NMR tube, dissolved in $CDCl_3$ and the resulting solution maintained at 55 °C for 34 h. The

https://doi.org/10.1021/acs.joc.3c01839
J. Org. Chem. XXXX, XXX, XXX−XXX

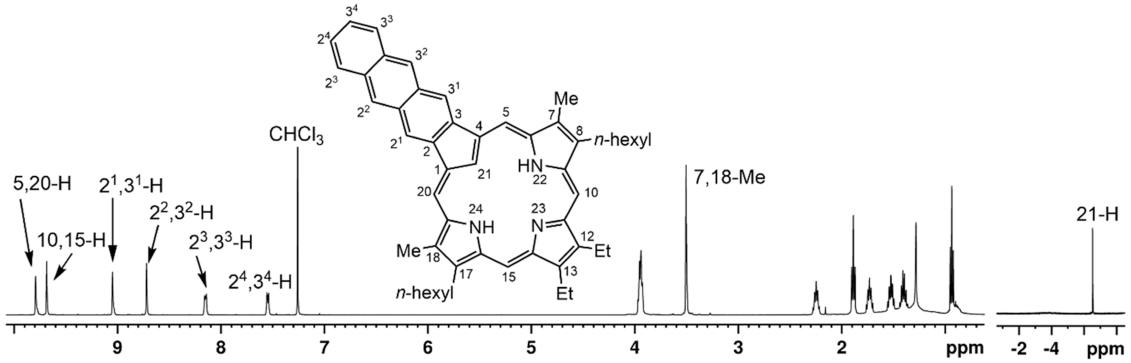

Figure 4. 500 MHz proton NMR spectrum of anthrocarbaporphyrin **8** in $CDCl_3$ at 55 °C.

Scheme 4. Metalation of Anthrocarbaporphyrin 8

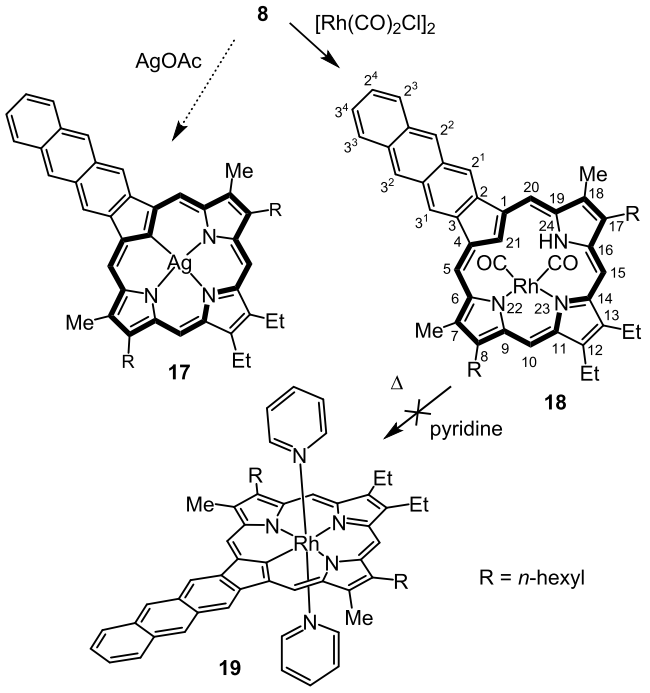

conversion occurred cleanly, and no other species could be identified. Proton NMR spectra were collected periodically, and the percentage compositions of **21** and **22** were determined by comparing the integrations for the internal methyl group. The results of this time course study are shown in Figure 7, and this shows that 50% conversion of intermediate **21** to C-methyl product **22** took approximately 33 h.

The proton NMR spectrum of *N*-methyl complex **21** showed that it fully retained the aromatic characteristics of the parent anthrocarbaporphyrin and the external *meso*-protons gave rise to four downfield singlets between 10.2 and 9.6 ppm (Figure 8A). The anthracene protons closest to the macrocycle (2^1,3^1-H) also gave two 1H singlets between 9.0 and 8.9 ppm due to deshielding by the adjacent porphyrinoid ring current. The internal *N*-methyl group was similarly shifted upfield to −2.5 ppm. The UV−vis spectrum for the complex gave a porphyrin-like Soret band at 477 nm and a series of Q bands between 600 and 700 nm (Figure 9).

The spectroscopic data for rearranged complex **22** were dramatically altered. Proton NMR spectroscopy confirmed that **22** had regained a plane of symmetry and the presence of a diamagnetic ring current was evident. However, the diatropic character of **22** appears to be considerably reduced as the *meso*-protons now give two 2H singlets at 9.55 and 8.84 ppm, values that represent ca. 0.7 ppm upfield shifts compared to the values for **21** (Figure 8B). The internal methyl group resonance appeared at −1.45 ppm, but when the fact that the substituent is no longer connected to an electronegative nitrogen is taken into account, the upfield shift is again substantially reduced compared to **21**. Similar palladium(II) complexes of carbaporphyrin **23**,[25] benzocarbaporphyrin **6**,[10,24] and naphthocarbaporphyrin **24**[17] have previously been described and a comparison of the spectroscopic results for this series provided unexpected insights (Table 2). Benzocarbaporphyrin complex **6** can potentially take on a 22π electron conjugation pathway that competes with the usual 18π electron porphyrinoid circuit. Similarly, **24** may provide access to a 26π electron route while anthracarbaporphyrin derivative **22** can support a 30π electron pathway. Hence, expanded aromatic pathways become increasing accessible with further ring fusion.

Nevertheless, the proton NMR data unambiguously show that the diatropicity of these systems decreases with increasing π-conjugation (Table 2). C-Methyl carbaporphyrin complex **23** showed *meso*-proton resonances at 10.42 and 10.00 ppm, but these values are reduced to 10.27 and 9.56 in benzo-fused complex **6**, 9.85 and 9.13 ppm in naphthalene-fused complex **24**, and 9.54 and 8.84 ppm in the new anthracene-fused complex **22**. It is particularly striking that the 5,20-protons in **23** are further downfield than the other complexes even though they are not next to a deshielding fused benzenoid unit. External methyl substituents in porphyrins are commonly deshielded by the strong macrocyclic ring current, resonating near 3.6 ppm, and this can also be used as a measure of the diatropicity for these systems. These resonances shift from 3.49 ppm in **23** to 3.03 ppm in **22**, lending further support to the notion that the aromatic properties decrease across the series (Table 2). More dramatically, the internal C-methyl in **23** appears at −4.46 ppm[25] but is shifted upfield by 3 ppm in anthracene complex **22**. It is more difficult to assess the effects on the fused benzenoid protons, but some downfield shifts are evident. As the ring currents appear to be undermined by expanding the π-system, the minimal shifts seen for anthracene protons in complex **22** are to be expected. The UV−vis spectrum of **22** is very different from *N*-methyl complex **21**, showing a weakened Soret band at 348 and 449 nm, and strongly red-shifted absorptions at 762 and 841 nm. A comparison of the UV−vis spectra of complexes **6**, **23**, and **22** is insightful (Figure 10). The Soret-like bands underwent minor shifts with increasing conjugation but the broad absorptions at longer wavelengths were dramatically shifted going from benzo-complex **6** (697 nm) to naphtho-

https://doi.org/10.1021/acs.joc.3c01839
J. Org. Chem. XXXX, XXX, XXX−XXX

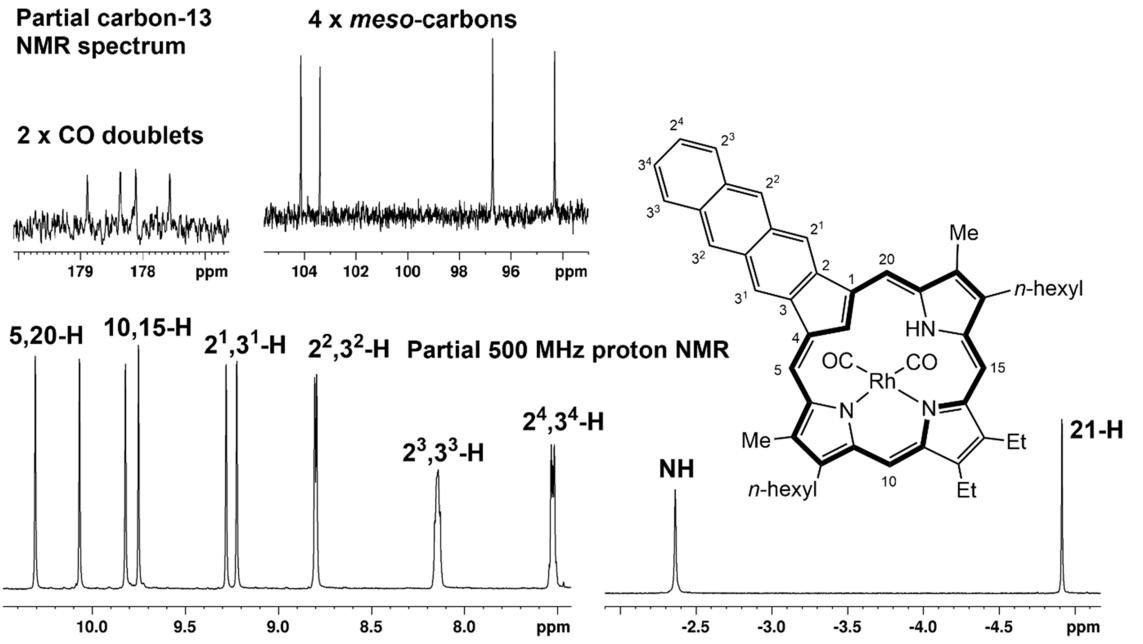

Figure 5. Partial proton NMR spectrum of rhodium(I) anthrocarbaporphyrin **18** in $CDCl_3$ at 55 °C showing the downfield and upfield regions. Inset: partial carbon-13 NMR spectrum showing the ^{107}Rh-coupled doublets for the carbonyl units and the four *meso*-carbon resonances near 100 ppm.

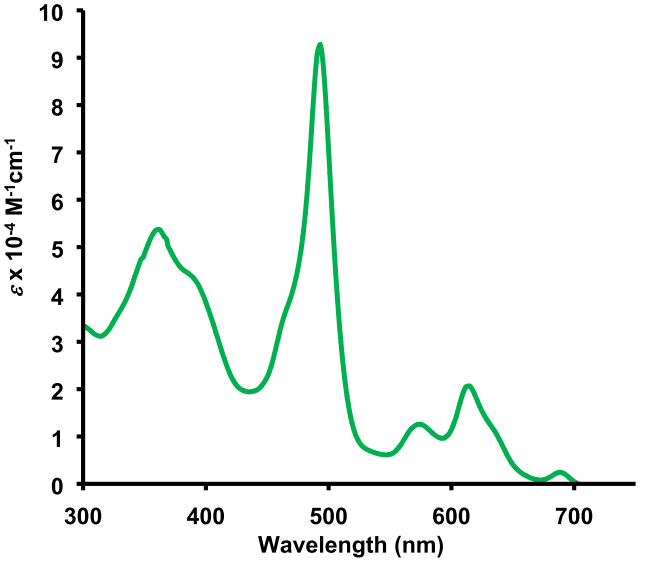

Figure 6. UV−vis spectrum of rhodium(I) anthrocarbaporphyrin **18** in $CHCl_3$.

Scheme 5. Palladium Complexes of Anthrocarbaorphyrin

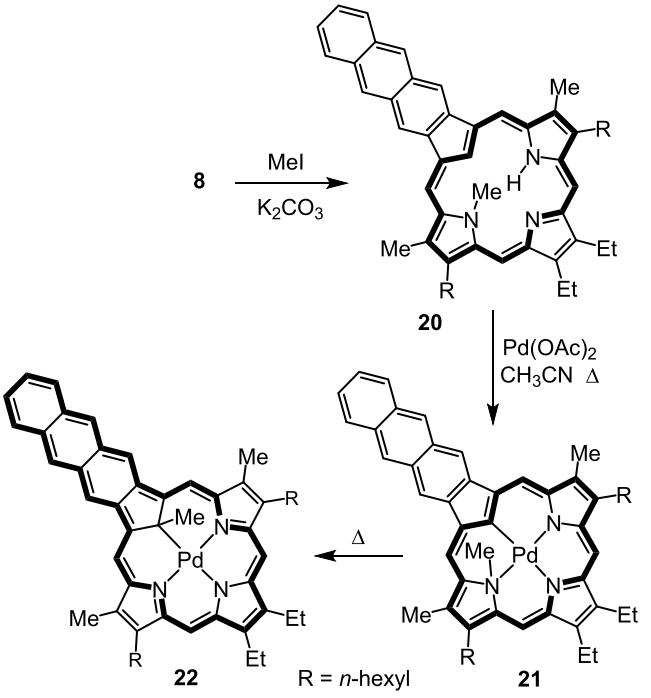

complex **24** (772 nm) to anthro-derivative **22** (842 nm), providing strong evidence for the presence of an expanded chromophore.

Computational Studies. To gain a better understanding on how ring fusion affects the aromatic characteristic of anthrocarbaporphyrins (ACPs), density functional theory (DFT) calculations[26−30] were carried out on four tautomers of unsubstituted anthro[2,3-*b*]-21-carbaporphyrin, three monoprotonated species and a diprotonated dication (Table 3). The structures were optimized using M06-2X with the triple-ζ basis set 6-311++G(d,p). In the free base tautomers, two protons are moved around within the cavity (positions 21, 22, 23, and 24) and are designated as **ACP-22,24-H**, **ACP-22,23-H**, **ACP-21,23-H**, and **ACP-21,22-H** to emphasize these differences. The monocations have an additional internal proton and are labeled similarly, but only one dicationic form, **ACPH**$_2^{2+}$, was considered (Table 3). The relative stabilities of these structures were assessed and the relative Gibbs free energies were also determined. Tautomer **ACP-22,24-H** was found to be the most stable, although **ACP-22,23-H** was only ca. 5 kcal/mol higher in energy (Table 3). The latter species is less favored because the internal hydrogens in **ACP-22,24-H** are better situated for hydrogen-bonding interactions, tautomers **ACP-21,23-H** and **ACP-21,22-H** have internal methylene units and are significantly less stable even though they retain 18π electron delocalization pathways. In addition, the two more stable

https://doi.org/10.1021/acs.joc.3c01839
J. Org. Chem. XXXX, XXX, XXX−XXX

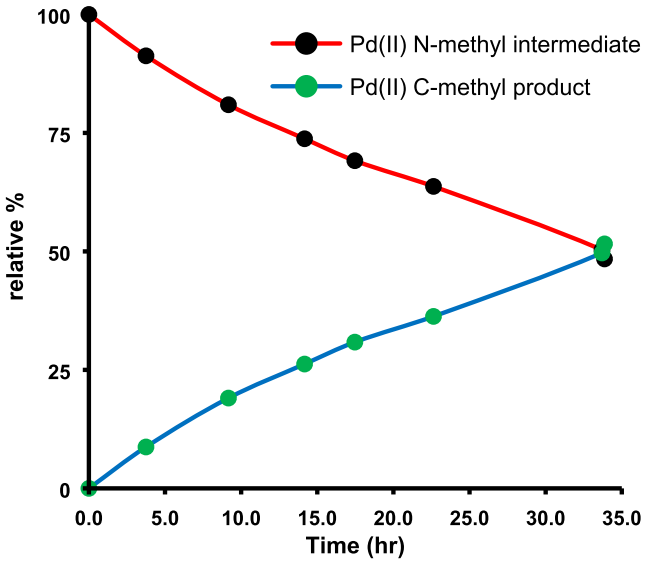

Figure 7. Time course experiment showing the rate of conversion of intermediary palladium(II) complex **21** to C-methyl derivative **22** in $CDCl_3$ at 55 °C.

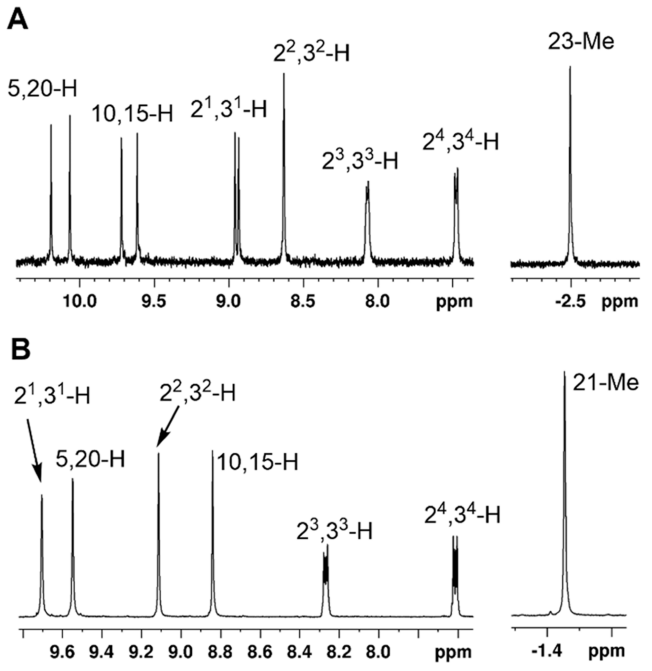

Figure 8. Partial proton NMR spectra of palladium(II) complexes **21** (A) and **22** (B).

tautomers are significantly distorted, while the less stable tautomers are virtually planar (Table 4). **ACP-21,23-H** was calculated to be ca. 10 kcal/mol higher in energy than **ACP-22,24-H**, but **ACP-21,22-H** is destabilized by nearly 20 kcal/mol. The latter structure places two nitrogen lone pairs adjacent to one another, and is slightly more sterically crowded, and this explains the difference in stability. Earlier calculations for carbaporphyrins, benzocarbaporphyrins, and naphthocarbaporphyrins have shown that tautomers with internal CH_2 units are less favored even though the cavity of **ACP- 21,23-H** is not sterically crowded.[17,31,32]

Nucleus-independent chemical shift (NICS) calculations[33] were performed to determine the diatropic character of these

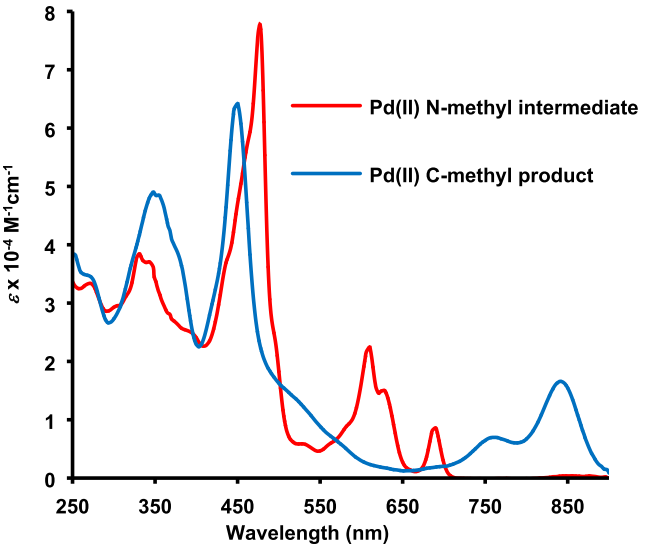

Figure 9. UV−vis spectra of *N*-methyl palladium(II) complex **21** (red) and C-methyl complex **22** (blue) in $CDCl_3$.

tautomers (Table 3). In NICS calculations, a large negative value within the macrocyclic cavity signifies aromatic character, while a large positive result may indicate antiaromaticity. Values close to zero indicate that the system is nonaromatic. Standard NICS calculations consider the effects due to σ and π electrons and are not always accurate.

However, $NICS_{zz}$ calculations primarily measure the effects due to the π system and are generally more reliable. In this work, NICS and $NICS_{zz}$ calculations were carried out; the latter calculations were performed 1 Å above the ring ($NICS(1)_{zz}$). Although the values obtained using $NICS(1)_{zz}$ are much larger than those for standard NICS calculations, the same trends were noted using both methods. In the discussion, the results obtained using $NICS(1)_{zz}$ calculations will primarily be used to avoid confusion. The NICS and $NICS(1)_{zz}$ values for tautomers with an internal methylene group gave very small negative values, demonstrating that these structures are only weakly diatropic. On the other hand, **ACP-22,24-H** and **ACP-22,23-H** gave large negative $NICS_{zz}$ values of −34.40 and −33.24 ppm, respectively, showing that these structures are strongly aromatic (Table 3). The NICS and $NICS(1)_{zz}$ values for the individual rings (a−g) were also calculated and these provide insights into the favored delocalization pathways for these systems. In **ACP-22,24-H**, the results are consistent with a conventional 18π electron delocalization pathway. Ring *a* gave a $NICS(1)_{zz}$ value of +10.77 ppm, demonstrating that the center of this ring lies outside of the global aromatic circuit. Similar results were obtained for **ACP-22,23-H**. However, in tautomers **ACP-21,23-H** and **ACP-21,22-H** with internal CH_2 units, ring *a* gave $NICS(1)_{zz}$ values of −7.43 and −8.12 ppm, implying that this ring falls inside the overall aromatic circuit. These tautomers can potentially possess 18π, 22π, 26π, and 30π electron delocalization pathways illustrated for **ACP-21,23-H** in Figure 11. The NICS data suggest that resonance contributor **ACP-21,23-H**$^{30\pi}$ dominates as the NICS values for rings e, f, and g give large negative values that are consistent with the aromatic pathway extending around the periphery of the fused anthracene unit. Further evidence for the 30π electron circuit being the favored pathway was confirmed using anisotropy of induced current density (AICD).[34,35] The AICD plot for **ACP-22,24-H** indicates that a porphyrin-like 18π electron pathway is favored,

https://doi.org/10.1021/acs.joc.3c01839
J. Org. Chem. XXXX, XXX, XXX−XXX

Table 2. Selected Proton NMR Resonances for Palladium(II) Annulated Carbaporphyrins Illustrating the Decrease in Diatropic Character as the π-System is Extended

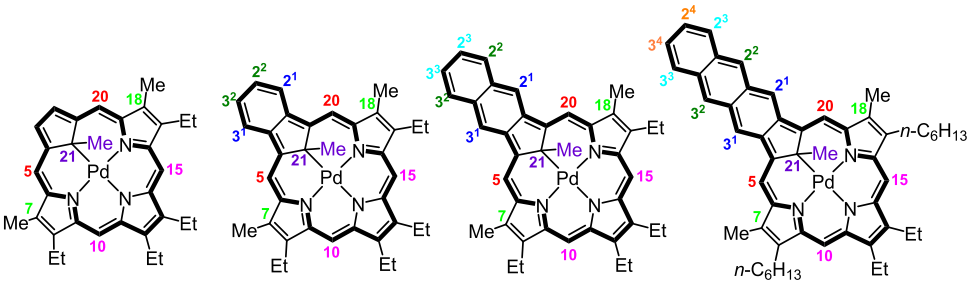

	23[25]	**6**	**24**	**22**
$2^4,3^4$-H	-	-	-	7.64-7.60
$2^3,3^3$-H	-	-	7.84-7.81	8.29-8.25
$2^2,3^2$-H	-	8.26-8.22	8.54-8.50	9.11
$2^1,3^1$-H	-	9.43-9.40	9.69	9.71
5,20-H	10.42	10.27	9.85	9.54
10,15-H	10.00	9.56	9.13	8.84
7,18-Me	3.49	3.33	3.16	3.03
21-Me	-4.46	-3.51	-2.18	-1.46

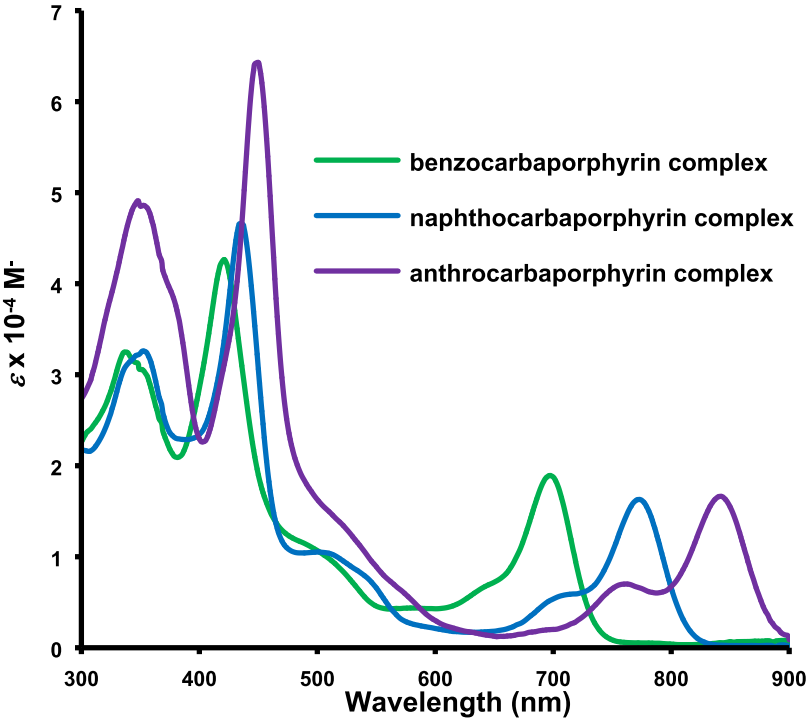

Figure 10. UV−vis spectra of palladium(II) complexes **6**, **24**,[10] and **22**.[17]

but a 30π electron pathway is clearly evident for **ACP-21,23-H** (Figure 12).

Three fully conjugated monocations were considered, two of which have internal methylene units (Table 3). **ACP-22,23,24-H**$^+$ was the least planar but the most stable of the three. However, **ACP-21,22,24-H**$^+$ proved to be only 4.65 kcal/mol higher in energy, while **ACP-21,22,23-H**$^+$ was 8.43 kcal/mol less stable. The arrangement of core atoms in **ACP-21,22,24-H**$^+$ facilitates more favorable hydrogen-bonding interactions than **ACP-21,22,23-H**$^+$, but the inner CH_2 unit does not undermine the stability of the system to the same extent as the free base structures. NICS calculations show that cation **ACP-22,23,24-H**$^+$ is fully aromatic and demonstrates that a 19-atom 18π electron delocalization pathway is favored (Figure 13). Rings b, c, and d give strongly negative NICS values, while ring a afforded positive values. The AICD plot for **ACP-22,23,24-H**$^+$ also confirms this assignment (Figure 14). The aromatic character of **ACP-21,22,24-H**$^+$ and **ACP-21,22,23-H**$^+$ is much reduced even though these structures favor 31-atom 30π electron conjugation pathways (Figure 13). Dication **ACPH**$_2^{2+}$ has an interior methylene group and can take on 18, 22, 26, and 30π electron conjugation pathways (Scheme 3). However, NICS calculations show that this species is only weakly diatropic (Table 3). Rings a−g all demonstrate significant negative $NICS_{zz}$ values and this

https://doi.org/10.1021/acs.joc.3c01839
J. Org. Chem. XXXX, XXX, XXX−XXX

Table 3. Calculated Relative Energies and NICS Values for Anthrocarbaporphyrin Tautomers and Related Protonated Species

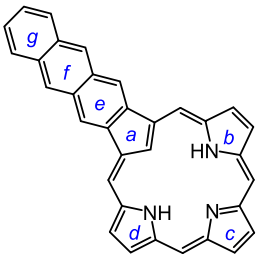

ACP_05

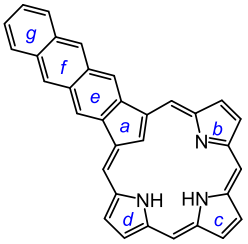

ACP_06

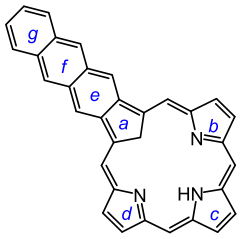

ACP_07

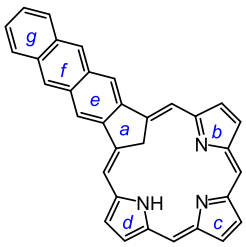

ACP_08

ΔG298 (kcal/mol)	0.00	4.86	9.79	17.31
ΔE(kcal/mol)	0.00	5.32	11.66	19.19
NICS(0)	−13.77	−13.42	−02.33	−02.65
NICS(01)$_{zz}$	**−34.40**	**−33.24**	**−03.51**	**−03.96**
NICS(a)	+06.80	+06.82	−00.40	−01.06
NICS(a1)$_{zz}$	**+10.77**	**+33.98**	**−07.43**	**−08.12**
NICS(b)	−13.19	+03.75	−02.12	−00.87
NICS(b1)$_{zz}$	**−31.34**	**−12.33**	**−11.31**	**−09.13**
NICS(c)	−04.35	−13.45	−10.84	−03.40
NICS(c1)$_{zz}$	**−21.06**	**−28.22**	**−26.28**	**−14.10**
NICS(d)	−13.19	−13.87	−02.12	−10.93
NICS(d1)$_{zz}$	**−31.34**	**−42.33**	**−11.31**	**−26.16**
NICS(e)	−04.71	+04.37	−09.13	−09.33
NICS(e1)$_{zz}$	**−15.54**	**−13.33**	**−27.86**	**−28.18**
NICS(f) **NICS(f1)$_{zz}$**	−10.37 **−31.03**	−10.21 **−30.16**	−11.97 **−35.49**	−12.05 **−35.65**
NICS(g)	−06.94	−07.45	−07.14	−07.17
NICS(g1)$_{zz}$	**−24.57**	**−22.97**	**−24.51**	**−24.57**

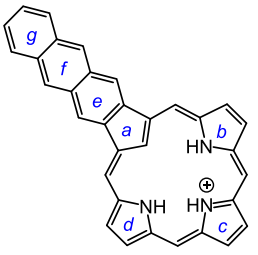

ACP_09

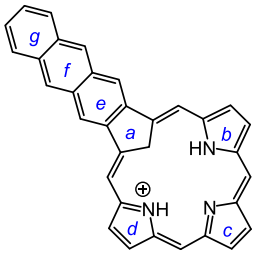

ACP_10

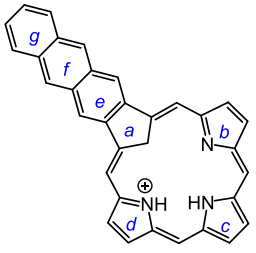

ACP_11

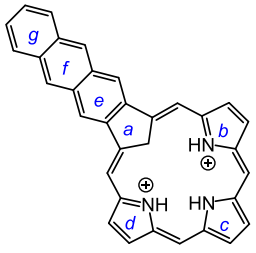

ACP_12

ΔG298 (kcal/mol)	0.00	3.01	7.04	
ΔE(kcal/mol)	0.00	4.65	8.43	
NICS(0)	−12.70	−05.35	−03.69	−02.66
NICS(01)$_{zz}$	**−29.68**	**−10.65**	**−06.77**	**−03.33**
NICS(a)	+09.91	−04.01	−02.22	−00.64
NICS(a1)$_{zz}$	**+17.63**	**−15.13**	**−10.91**	**−06.27**
NICS(b)	−12.98	−09.72	+00.06	−07.37
NICS(b1)$_{zz}$	**−25.23**	**−24.41**	**−06.75**	**−15.21**
NICS(c)	−14.92	−04.98	−10.33	−10.43
NICS(c1)$_{zz}$	**−48.16**	**−17.58**	**−26.64**	**−29.34**
NICS(d)	−12.98	−09.72	−10.11	−07.37
NICS(d1)$_{zz}$	**−25.20**	**−24.42**	**−20.91**	**−15.21**
NICS(e)	−03.30	−11.35	−10.46	−11.57
NICS(e1)$_{zz}$	**−11.07**	**−33.32**	**−31.15**	**−34.68**
NICS(f)	−09.56	−13.61	−13.21	−16.22
NICS(f1)$_{zz}$	**−28.98**	**−39.94**	**−38.69**	**−47.27**
NICS(g)	−07.21	−08.00	−07.90	−10.61
NICS(g1)$_{zz}$	**−25.71**	**−27.18**	**−26.86**	**−34.80**

indicates that a 32-atom 30π-electron pathway that runs around the periphery of the anthracene unit is favored (Figure 13). The AICD plot for the dication also shows the presence of this conjugation pathway (Figure 14).

Although tautomers **ACP-21,23-H** and **ACP-21,22-H** are not favored, C-methyl palladium(II) complex **22** essentially represents a trapped version of these conjugation pathways. As the observed diatropicity of the palladium complexes decreases with increasing conjugation, insights can be obtained by comparing NICS calculations for carbaporphyrin tautomer **CP-21,23-H**, benzocarbaporphyrin **BCP-21,23-H**, naphthocarbaporphyrin **NCP-21,23-H**, and anthrocarbaporphyrin **ACP-**

https://doi.org/10.1021/acs.joc.3c01839
J. Org. Chem. XXXX, XXX, XXX−XXX

Table 4. Calculated Dihedral Angles for Anthrocarbaporphyrins and Related Protonated Species

	dihedral angles				
molecule	ab	bc	cd	da	average
ACP-22,24-H	−12.69	2.42	−2.41	12.67	7.55
ACP-22,23-H	7.66	−1.89	7.82	−14.04	7.85
ACP-21,23-H	0.00	−0.01	0.01	0.00	0.01
ACP-21,22-H	0.00	0.00	0.00	0.00	0.00
ACP-22,23,24-H$^+$	18.98	####	####	−19.00	16.89
ACP-21,22,24-H$^+$	0.00	0.00	0.00	0.00	0.00
ACP-21,22,23-H$^+$	1.07	3.19	−9.25	7.67	5.30
ACPH$_2^{2+}$	7.50	####	####	−7.50	12.72
CP-21,23-H	0.00	0.00	0.00	0.00	0.00
BCP-21,23-H	−0.01	0.01	−0.01	0.01	0.01
NCP-21,23-H	0.00	−0.02	0.02	0.00	0.01

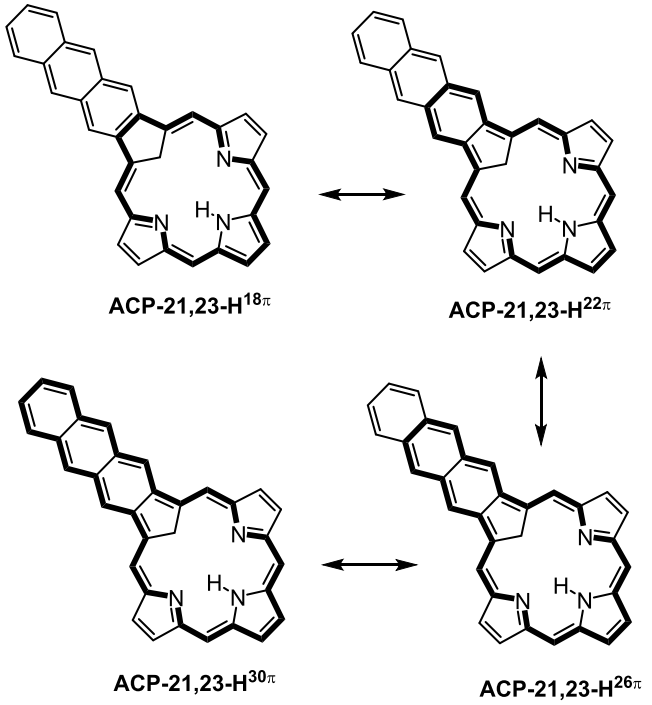

Figure 11. Potential aromatic delocalization pathways for **ACP-21,23-H**.

21,23-H (Table 5). **CP-21,23-H** is strongly aromatic with a NICS(1)$_{zz}$ value of −25.58 ppm but this is approximately halved for **BCP-21,23-H** and halved again for **NCP-21,23-H**. For **ACP-21,23-H**, NICS(1)$_{zz}$ was calculated to be only −3.51 ppm. Although this trend mirrors the one noted earlier for palladium(II) complexes **23**, **6**, **22**, and **24**, the diminished ring currents predicted for highly conjugated structures of this type seemingly exaggerate the case. This may be due in part to the altered conformation of the palladium(II) complexes compared to the related nonmetalated tautomers. The calculated conformations for **PdCP**, **PdBCP**, **PdNCP**, and **PdACP** are relatively planar (Figure 15), in good agreement with the X-ray structure for a palladium(II) complexes of a benzocarbaporphyrin.[11] As the palladium cation occupies the center of the macrocycle, it was not possible to calculate NICS(0) values, but the individual rings could be assessed. Focusing in on ring *a*, which forms a critical junction between the anthracene and carbaporphyrin components, going from

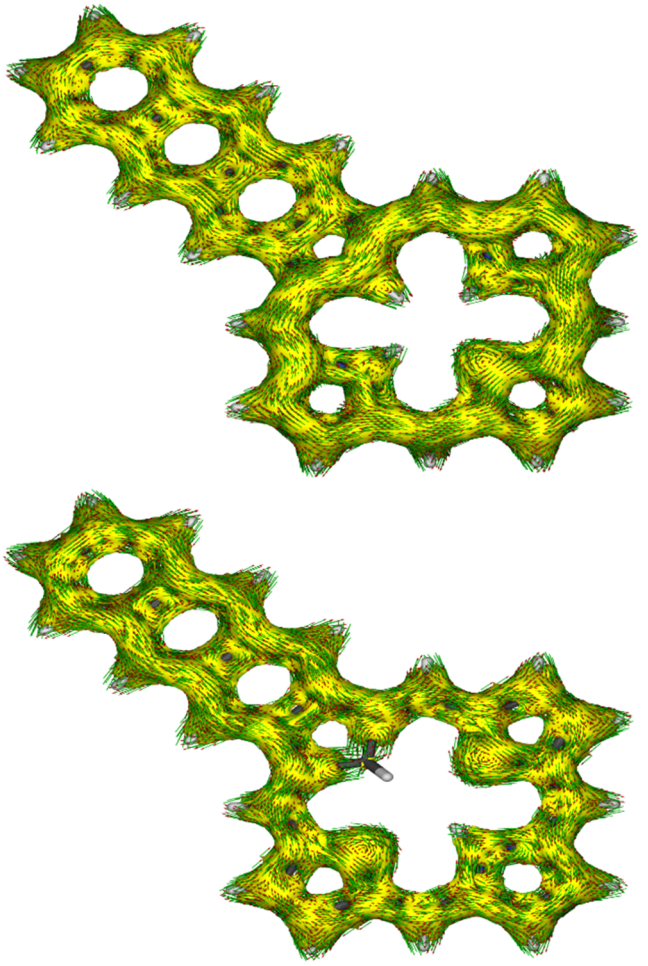

Figure 12. AICD plots (isovalues = 0.05) of anthrocarbaporphyrin tautomers **ACP-22,24-H** (top) and **ACP-21,23-H** (bottom).

CP-21,23-H to **ACP-21,23-H**, NICS(a) drops from −12.74 to −0.40 ppm. A similar but more gentle decline is noted for palladium complexes **Pd-CP**, **PdBCP**, **PdNCP**, and **PdACP** drops from −15.20 to −2.23 ppm (Table 6). Therefore, the computational data appear to be fully consistent with the experimental results. AICD plots for these complexes also confirm the presence of conjugation pathways that encompass the fused aromatic rings, and this is illustrated for **PdACP** in Figure 16.

CONCLUSIONS

The "3 + 1" variant on the MacDonald condensation has been used to prepare novel anthrocarboporphyrins. The carbaporphyrin core is fully aromatic, but the fused anthracene unit is not directly involved in global π-delocalization. Addition of TFA initially afforded a monoprotonated species, but at higher concentrations, a C-protonated dication was formed. UV−vis spectroscopy and DFT studies indicate that the latter species has an extended 32-atom 30π electron delocalization pathway. Reaction with methyl iodide and potassium carbonate afforded a *N*-methyl derivative and this reacted with palladium(II) acetate to give an organometallic complex that retained similar aromatic properties to free base anthrocarbaporphyrin. Upon heating, the methyl group of the initial palladium(II) complex migrated onto the internal carbon atom. The resulting UV−vis spectrum showed large bathochromic shifts due to the expansion of the π-

https://doi.org/10.1021/acs.joc.3c01839
J. Org. Chem. XXXX, XXX, XXX−XXX

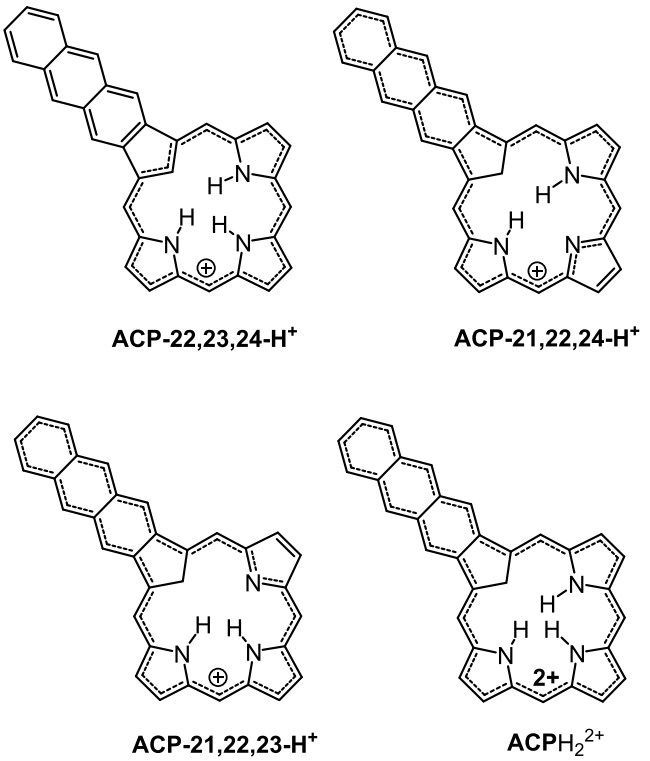

Figure 13. Aromatic delocalization pathways in protonated anthrocarbaporphyrins.

electron delocalization pathway. Nevertheless, when comparing carbaporphyrins with fused benzene, naphthalene, and anthracene units, the diatropic character dramatically decreases as the conjugation pathway increases. NICS calculations and AICD plots confirmed these observations. This study provides valuable insights into the effects caused by expanding the π-systems of porphyrinoid systems.

EXPERIMENTAL SECTION

Melting points are uncorrected. NMR spectra were recorded using a 400 or 500 MHz NMR spectrometer and were run at 302 K unless otherwise indicated. ^{1}H NMR values are reported as chemical shifts δ, relative integral, multiplicity (s, singlet; d, doublet; t, triplet; q, quartet; m, multiplet; br, broad peak), and coupling constant (J). Chemical shifts are reported in parts per million (ppm) relative to $CDCl_3$ (^{1}H residual $CHCl_3$ δ 7.26, ^{13}C $CDCl_3$ triplet δ 77.23) or d_6-DMSO (^{1}H residual d_5-DMSO pentet δ 2.49, ^{13}C d_6-DMSO heptet δ 39.7), and coupling constants were taken directly from the spectra. NMR assignments were made with the aid of ^{1}H−^{1}H COSY, HSQC, DEPT-135, and NOE difference proton NMR spectroscopy. 2D experiments were performed by using standard software. High-resolution mass spectra (HRMS) were carried out by using a double-focusing magnetic sector instrument. ^{1}H and ^{13}C{^{1}H} NMR spectra for all new compounds are reported in the Supporting Information.

Caution. THF was freshly distilled from calcium hydride to remove traces of peroxides. Trifluoroacetic acid should be handled in a well-ventilated fume hood.

***endo*-1,4-Methano-1,2,3,4-tetrahydro-2,3-dihydroxynaphthacene (14).** A solution of tetra-*n*-butylammonium permanganate (1.212 g, 7.67 mmol) in dichloromethane (50 mL) was added to a stirred mixture of 3,9 M aqueous sodium hydroxide (0.32 mL) and 1,4-methano-1,4-dihydronaphthacene[19] (**13**, 500 mg, 2.066 mmol) in dichloromethane (35 mL) while maintaining the temperature at 0 °C with the aid of a salt-ice bath. The mixture was stirred at 0 °C for 20 min and quenched with a saturated solution of sodium metabisulfite (4 mL). The mixture was extracted with ethyl acetate (6 × 50 mL), dried over magnesium sulfate, and the solvent removed on a rotary evaporator. The residue was dissolved in ethyl acetate, transferred into a 50 mL round-bottom flask, and reevaporated. The residue was heated with chloroform (10 mL), cooled, and filtered to give the dialcohol (182 mg, 0.659 mg, 32%) as an off-white solid, mp > 260 °C. ^{1}H NMR (500 MHz, $CDCl_3$): δ 8.39 (s, 2H), 8.02−7.99 (m, 2H), 7.77 (s, 2H), 7.46−7.43 (m, 2H), 4.94−4.92 (br d, 2H), 3.73−3.70 (m, 2H), 3.26 (br t, 2H, J = 2 Hz), 2,30 (dt, 1H, J = 1,5, 9.5 Hz), 1.77 (dp, 1H, J = 9.5, 1.5 Hz). ^{13}C{^{1}H} NMR (125 MHz, $CDCl_3$): δ 143.6, 131.1, 130.8, 127.6, 125.3, 124.9, 118.9, 71.2, 50.1, 40.5. HRMS (ESI-TOF) m/z: M^+ calcd for $C_{19}H_{16}O_2$ 276.1150; Found 276.1147.

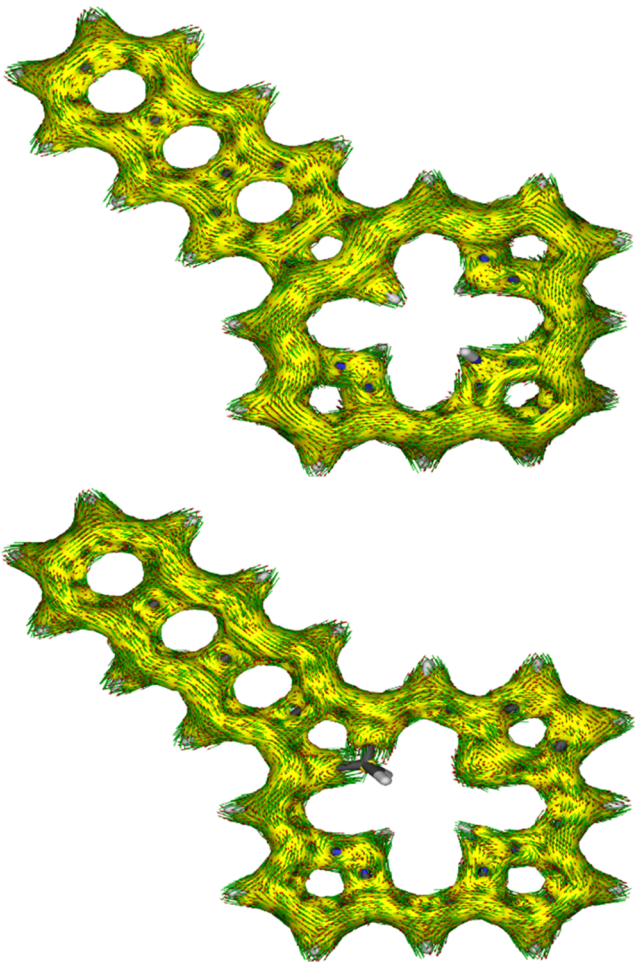

Figure 14. AICD plots (isovalues = 0.05) of anthrocarbaporphyrin cation **ACP-22,23,24-H**$^+$ (top) and dication **ACPH**$_2^{2+}$ (bottom).

***cis*-Naphtho[2,3-*f*]Indane-1,3-dicarbaldehyde (9).** A suspension of potassium periodate (200 mg, 0.87 mmol) in water (6 mL) was added to a solution of the foregoing diol (175 mg, 0.634 mmol) in THF (15 mL) and the mixture was stirred vigorously at room temperature for 90 min. The mixture was extracted with ethyl acetate (x3) and the organic solutions were dried over sodium sulfate. Evaporation of the solvent gave the dialdehyde (156 mg, 0.57 mmol, 90%) as a light brown solid, mp 132−134 °C, dec (softened at 120 °C). The product could be stored in the freezer for several months without appreciable decomposition. ^{1}H NMR (500 MHz, $CDCl_3$): δ 9.81 (d, 2H, J = 2.3 Hz), 8.41 (s, 2H), 8.02−7.99 (m, 2H), 7.97 (s, 2H), 7.50−7.47 (m, 2H), 4.21 (t, 2H, J = 7.2 Hz), 2.96 (dt, 1H, J = 13.7, 5.9 Hz), 2.66 (dt, 1H, J = 13.7, 8.9 Hz). ^{13}C{^{1}H} NMR (125 MHz, $CDCl_3$): δ 199.3, 136.8, 132.1, 131.6, 128.3, 126.6, 126.0, 125.0, 56.2, 26.2. HRMS (ESI-TOF) m/z: M^+ calcd for $C_{19}H_{14}O_2$ 274.0994; Found 274.0990.

12,13-Diethyl-8,17-dihexyl-7,18-dimethylanthro[2,3-*b*]-carbaporphyrin (8). Tripyrrane dicarboxylic acid **15**[21] (75.2 mg, 0.13 mmol) was stirred with trifluoroacetic acid (1 mL) under nitrogen for 1

https://doi.org/10.1021/acs.joc.3c01839
J. Org. Chem. XXXX, XXX, XXX−XXX

Table 5. Calculated NICS Values for Palladium(II) Carbaporphyrin Complexes

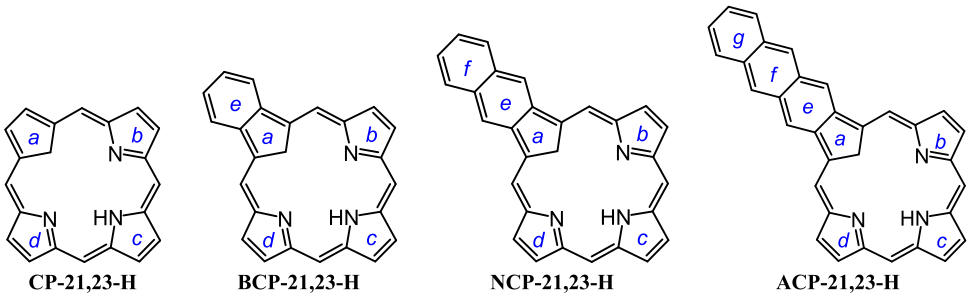

	CP-21,23-H	BCP-21,23-H	NCP-21,23-H	ACP-21,23-H
NICS(0)	−10.41	−05.51	−03.42	−02.33
NICS(01)$_{zz}$	**−25.58**	**−12.21**	**−06.54**	**−03.51**
NICS(a)	−12.74	−05.18	−01.97	−00.40
NICS(a1)$_{zz}$	**−40.08**	**−19.86**	**−11.55**	**−07.43**
NICS(b)	−01.50	−01.88	−02.02	−02.12
NICS(b1)$_{zz}$	**−11.34**	**−11.35**	**−11.30**	**−11.31**
NICS(c)	−13.17	−11.93	−11.24	−10.84
NICS(c1)$_{zz}$	**−33.83**	**−29.69**	**−27.52**	**−26.28**
NICS(d)	−1.50	−01.88	−02.02	−02.12
NICS(d1)$_{zz}$	**−11.34**	**−11.35**	**−11.30**	**−11.31**
NICS(e)		−08.84	−10.40	−09.13
NICS(e1)$_{zz}$		**−29.29**	**−31.36**	**−27.86**
NICS(f)			−08.47	−11.97
NICS(f1)$_{zz}$			**−27.96**	**−35.49**
NICS(g)				−07.14
NICS(g1)$_{zz}$				**−24.51**

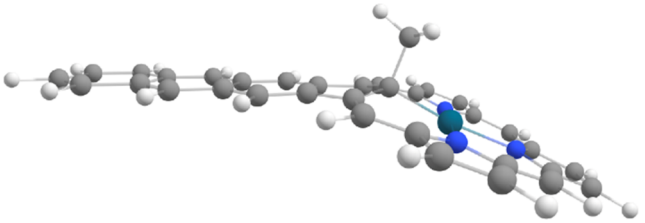

Figure 15. Calculated conformation for palladium(II) complex PdACP.

min. The mixture was diluted with dichloromethane (50 mL), anthracene dialdehyde **9** (34.3 mg, 0.13 mmol) was immediately added, and the mixture was stirred for 16 h under nitrogen. The resulting solution was neutralized with triethylamine and oxidized by stirring with DDQ (59 mg, 0.26 mmol) for 3 h. The mixture was washed with water and then with saturated sodium bicarbonate. The solvent was removed under reduced pressure and the residue chromatographed on a small column of grade 3 alumina eluting with dichloromethane. The product fraction was further purified by column chromatography on grade 2 alumina, eluting with 1:1 dichloromethane-hexanes, and the major dark red-brown band was collected. The solvent was removed under reduced pressure, and the residue was recrystallized from

Table 6. Calculated NICS Values for Pd(II) Carbaporphyrin Complexes

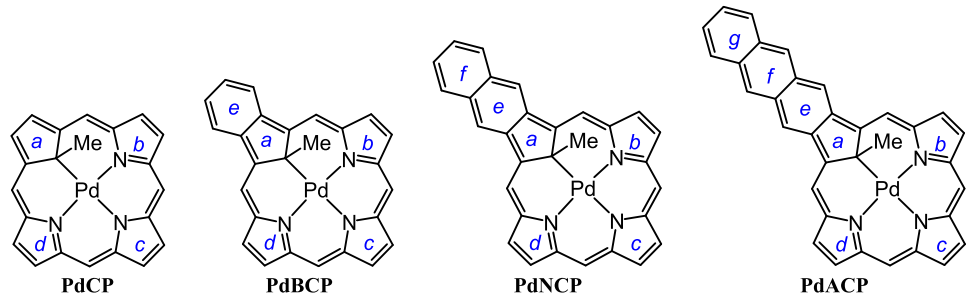

	PdCP	PdBCP	PdNCP	PdACP
NICS(a)	−15.20	−08.09	−04.23	−02.23
NICS(b)	−03.80	−03.39	−03.16	−03.01
NICS(c)	−05.25	−06.06	−06.16	−06.19
NICS(d)	−03.80	−03.39	−03.16	−03.01
NICS(e)		−08.93	−10.92	−09.81
NICS(f)			−08.62	−12.20
NICS(g)				−07.28

https://doi.org/10.1021/acs.joc.3c01839
J. Org. Chem. XXXX, XXX, XXX−XXX

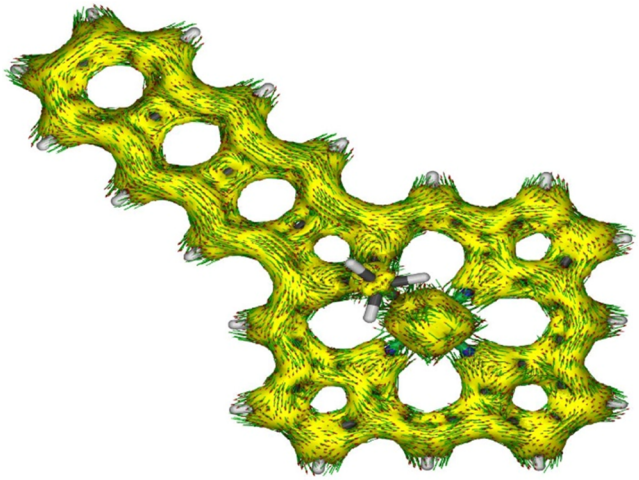

Figure 16. AICD plot (isovalue = 0.05) of **PdACP**.

chloroform−methanol to yield the anthrocarbaporphyrin (31.7 mg, 0.045 mmol, 36%) as a dark purple solid, mp > 300 °C. UV−vis ($CHCl_3$; 1.388×10^{-5} M): λ_{max}/nm (log ε) 401 (4.84), 426 (sh, 5.06), 448 (5.24), 492 (4.20), 531 (4.14), 569 (4.69), 615 (3.96), 677 (3.96). UV−vis (100 equiv TFA−$CHCl_3$; 1.388×10^{-5} M): λ_{max}/nm (log ε) 407 (sh, 4.90), 418 (4.95), 449 (4.94), 478 (5.08), 624 (4.54), 682 (3.88). UV−vis (50% TFA−$CHCl_3$; 1.388×10^{-5} M): λ_{max}/nm (log ε): 400 (4.84), 419 (4.83), 462 (4.58), 496 (4.70), 651 (4.30), 754 (4.20). ^{1}H NMR (500 MHz, $CDCl_3$): δ 9.79 (s, 2H, 5,10-H), 9.68 (s, 2H, 10,15-H), 9.05 (s, 2H, 2^1,3^1-CH), 8.72 (s, 2^2,3^2-CH), 8.16−8.14 (m, 2H, 2^3,3^3-CH), 7.56−7.54 (m, 2H, 2^4,3^4-CH), 3.97−3.93 (m, 8H, 12,13-CH_2 and 8,17-CH_2), 3.50 (s, 6H, 7,18-CH_3), 2.25 (p, 4H, J = 7.4 Hz, 8,17-CH_2CH_2), 1.89 (t, 6H, J = 7.7 Hz, 12,13- CH_2CH_3), 1.73 (p, 4H, J = 7.6 Hz, 8,17-$CH_2CH_2CH_2$), 1.52 (p, 4H, J = 7.4 Hz, 2 × $CH_2CH_2CH_3$), 1.40 (sextet, 4H, J = 7.4 Hz, 2 × $CH_2CH_2CH_3$), 0.93 (t, 6H, J = 7.3 Hz, 2 × $CH_2CH_2CH_3$), −6.54 (1H, s, 21-H). ^{13}C{^{1}H} NMR (125 MHz, $CDCl_3$): δ 152.2, 144.0, 141.2, 136.5, 135.9, 135.5, 134.3, 132.1, 128.6 (2^3,3^3-CH), 127.2 (2^2,3^2-CH), 125.4 (2^4,3^4-CH), 118.5 (2^1,3^1-CH), 116.84, 116.82, 96.3 (10,15-CH), 96.2 (5,20-CH), 32.9 (8,17-CH_2CH_2), 32.2 (2 × $CH_2CH_2CH_3$), 29.9 (8,17-$CH_2CH_2CH_2$), 26.4 (8,17-$CH_2CH_2CH_2$), 22.9 (2 × $CH_2CH_2CH_3$), 20.2 (12,13-CH_2), 18.6 (12,13-CH_2CH_3), 14.2 (2 × $CH_2CH_2CH_3$), 11.7 (7,18-CH_3). ^{1}H NMR (500 MHz, TFA-$CDCl_3$): δ 10.27 (s, 2H, 5,10-H), 10.02 (s, 2H, 10,15-H), 9.02 (br s, 2H, 2^1,3^1-CH), 8.55 (br s, 2^2,3^2-CH), 8.05−8.01 (m, 2H, 2^3,3^3-CH), 7.52−7.49 (m, 2H, 2^4,3^4-CH), 4.09 (q, 4H, J = 7.7 Hz, 12,13-CH_2), 4.04 (t, 4H, J = 7.8 Hz, 8,17-CH_2), 3.60 (s, 6H, 7,18-CH_3), 2.16 (p, 4H, J = 7.6 Hz, 2 × $CH_2CH_2CH_3$), 1.88 (t, 6H, J = 7.7 Hz, 12,13-CH_2CH_3), 1.70 (p, 4H, J = 7.5 Hz, 8,17-$CH_2CH_2CH_2$), 1.50 (p, 4H, J = 7.6 Hz, 2 × $CH_2CH_2CH_3$), 1.39 (sextet, 4H, J = 7.4 Hz, 2 × $CH_2CH_2CH_3$), 0.92 (t, 6H, J = 7.3 Hz, 2 × $CH_2CH_2CH_3$), −2.82 (s, 2H, 2 × NH), −4.20 (br s, 1H, NH), −6.23 (s, 1H, 21-H). ^{13}C{^{1}H} NMR (125 MHz, TFA-$CDCl_3$): δ 142.3, 141.1, 140.6, 140.2, 137.6, 136.3, 134.6, 132.5, 128.5 (2^3,3^3-CH), 127.8 (2^2,3^2-CH), 126.8, 125.9 (2^4,3^4-CH), 120.6 (2^1,3^1-CH), 102.1 (5,20-CH), 94.8 (10,15-CH), 32.5 (8,17-CH_2CH_2), 32.0 (2 × $CH_2CH_2CH_3$), 29.9 (8,17-$CH_2CH_2CH_2$), 26.8 (8,17-CH_2), 22.8 (2 × $CH_2CH_2CH_3$), 20.0 (12,13-CH_2), 17.6 (12,13-CH_2CH_3), 14.1 (2 × $CH_2CH_2CH_3$), 12.0 (7,18-CH_3). HRMS (ESI-TOF) m/z: M^+ calcd for $C_{51}H_{59}N_3$ 711.4552; Found 711.4531. HRMS (ESI-TOF) m/z: $[M + H]^+$ calcd for $C_{51}H_{58}N_3^+$ 712.4625; Found 712.4621.

Quinone 16. A minor green fraction eluted after the main product in the previous experiment. This product was not always observed, and the yield was less than 1% in all cases. UV−vis ($CHCl_3$): λ_{max}/nm (relative intensity) 348 (0.27), 407 (1.00), 453 (0.32), 477 (0.32), 591 (0.27), 624 (0.16). ^{1}H NMR (500 MHz, $CDCl_3$, 55 °C): δ 9.85 (s, 2H, 5,10-H), 9.67 (s, 2H, 10,15-H), 9.37 (s, 2H, 2^1,3^1-CH), 8.52−8.48 (m, 2H, 2^3,3^3-CH), 7.87−7.84 (m, 2H, 2^4,3^4-CH), 3.96 (t, 4H, J = 7.6 Hz, 8,17-CH_2), 3.90 (q, 4H, J = 7.7 Hz, 12,13-CH_2), 3.54 (s, 6H, 7,18-CH_3), 2.25 (p, 4H, J = 7.5 Hz, 8,17-CH_2CH_2), 1.87 (t, 6H, J = 7.7 Hz, 12,13-CH_2CH_3), 1.76−1.70 (m, 4H, 8,17-$CH_2CH_2CH_2$), 1.56−1.50 (m, 4H, 2 × $CH_2CH_2CH_3$), 1.42−1.36 (m, 4H, 2 × $CH_2CH_2CH_3$), 0.93 (t, 6H, J = 7.6 Hz, 2 × $CH_2CH_2CH_3$), −4.2 (v br, 2H, 2 × NH), −6.88 (s, 1H, 21-H). ^{13}C{^{1}H} NMR (125 MHz, $CDCl_3$): δ 184.1 (C=O),146.5, 141.7, 141.4, 139.9, 139.4, 138.1, 136.4, 134.4, 134.0, 133.9, 133.2 (2^4,3^4-CH), 127.3 (2^3,3^3-CH), 120.1 (2^1,3^1-CH), 111.8 (21-CH), 106.4 (5,20-CH), 95.2 (10,15-CH), 32.5 (8,17-CH_2CH_2), 32.0 (2 × $CH_2CH_2CH_3$), 29.9 (8,17-$CH_2CH_2CH_2$), 26.7 (8,17-CH_2), 22.8 (2 × $CH_2CH_2CH_3$), 20.0 (12,13-CH_2), 17.7 (12,13-CH_2CH_3), 14.2 (2 × $CH_2CH_2CH_3$), 12.1 (7,18-CH_3). ^{1}H NMR (500 MHz, trace TFA-$CDCl_3$): δ 10.63 (s, 2H, 5,10-H), 10.08 (s, 2H, 10,15-H), 9.70 (s, 2H, 2^1,3^1-CH), 8.30−8.27 (m, 2H, 2^3,3^3-CH), 7.71−7.68 (m, 2H, 2^4,3^4-CH), 4.11 (q, 4H, J = 7.7 Hz, 12,13-CH_2), 4.07 (t, 4H, J = 7.8 Hz, 8,17-CH_2), 3.67 (s, 6H, 7,18-CH_3), 2.18 (p, 4H, J = 7.4 Hz, 8,17-CH_2CH_2), 1.88 (t, 6H, J = 7.7 Hz, 12,13-CH_2CH_3), 1.69−1.63 (m, 4H, 8,17-$CH_2CH_2CH_2$), 1.50−1.44 (m, 4H, 2 × $CH_2CH_2CH_3$), 1.38−1.33 (m, 4H, 2 × $CH_2CH_2CH_3$), 0.90 (t, 6H, J = 7.3 Hz, 2 × $CH_2CH_2CH_3$), −2.78 (s, 2H, 2 × NH), −4.23 (br s, 1H, NH), −6.35 (s, 1H, 21-H). HRMS (ESI-TOF) m/z: $[M + H]^+$ calcd for $C_{51}H_{55}N_3O_2^+$ 742.4367; Found 742.4383.

12,13-Diethyl-8,17-dihexyl-7,18,21-trimethylanthro[2,3-*b*]carbaporphyrin (20). Anthrocarbaporphyrin **8** (20.2 mg, 0.028 mmol) was stirred with potassium carbonate (155.6 mg, 1.13 mmol) and methyl iodide (10 drops) in acetone (15 mL) under reflux for 16 h. The mixture was washed with water and evaporated under reduced pressure. The residue was run through a silica column, eluting with chloroform. The main green fraction was evaporated under reduced pressure, and the residue was recrystallized from chloroform−methanol to yield the *N*-methyl- carbaporphyrin **20** (10.1 mg, 0.0138 mmol, 49%), as purple crystals, mp 138−140 °C. UV−vis (1% Et_3N−$CHCl_3$; 1.386×10^{-5} M): λ_{max}/nm (log ε) 431 (sh, 4.92), 451 (5.10), 520 (4.09), 569 (4.37), 628 (3.82), 692 (3.64). UV−vis (10 equiv TFA-$CHCl_3$; 1.386×10^{-5} M): λ_{max}/nm (log ε) 423 (4.86), 462 (4.72), 492 (4.85), 641 (4.36), 700 (3.74). ^{1}H NMR (500 MHz, $CDCl_3$): δ 10.03 (s, 1H), 9.93 (s, 1H) (5,20-H), 9.66 (s, 1H), 9.51 (s, 1H) (10,15-H), 9.27 (s, 1H, s), 9.20 (s, 1H) (2^1,3^1-H), 8.81 (s, 1H), 8.79 (s, 1H) (2^2,3^2-H), 8.17−8.13 (m, 2H, 2^3,3^3-H), 7.54−7.51 (m, 2H, 2^4,3^4-H), 4.05−3.98 (m, 1H), 3.94−3.84 (m, 5H), 3.64 (t, 2H, J = 7.8 Hz) (8,12,13,17-CH_2), 3.58 (s, 3H) 3.22 (s, 3H) (7,18-CH_3), 2.26 (p, 2H, J = 7.6 Hz), 1.90−1.86 (m, 6H), 1.76 (p, 2H, J = 7.4 Hz), 1.67−1.50 (m, 4H), 1.42−1.31 (m, 6H, 12,13-CH_2CH_3), 0.94 (t, 3H, J = 7.3 Hz), 0.90 (t, 3H, J = 7.2 Hz) (8,17-CH_3), −2.33 (br s, 1H, 2 × NH), −3.99 (s, 3H, N−CH_3), −5.58 (s, 1H, 21-H). ^{1}H NMR (500 MHz, trace TFA−$CDCl_3$): 10.26 (s, 1H), 10.17 (s, 1H) (5,20-H), 9.99 (s, 1H), 9.92 (s, 1H) (10,15-H), 9.19 (s, 1H), 9.14 (s, 1H) (2^1,3^1-H), 8.74 (s, 2H, 2^2,3^2-H), 8.14−8.11 (m, 2H, 2^3,3^3-H), 7.57−7.54 (m, 2H, 2^4,3^4-H), 4.13−3.97 (m, 6H), 3.72−3.55 (m, 2H) (8,12,13,17-CH_2), 3.61 (s, 3H), 3.26 (s, 3H) (7,18-CH_3), 2.24−2.18 (m, 2H), 2.02−1.89 (m, 2H) (8,17-CH_2CH_2), 1.87 (t, 3H, J = 7.7 Hz), 1.81 (t, 3H, J = 7.7 Hz) (12,13-CH_2CH_3), 1.78−1.73 (m, 2H) 1.71−1.64 (m, 2H), 1.56−1.36 (m, 8H) (2 × $CH_2CH_2CH_2CH_3$), 0.95 (t, 3H, J = 7.3 Hz), 0.94 (t, 3H, J = 7.3 Hz), − 3.64 (br s, 1H, NH), −4.39 (s, 3H, N−CH_3), −5.94 (s, 1H, 21-H). ^{13}C{^{1}H} NMR (125 MHz, $CDCl_3$): δ 150.5, 148.5, 147.1, 144.4, 143.5, 143.1, 143.9, 142.6, 141.5, 141.2, 138.7, 135.1, 134.7, 134.6, 132.4, 132.3, 132.0, 131.8, 128.5 (2^3,3^3-CH), 127.9 (2^2,3^2-CH), 125.40, 125.36 (2^4,3^4-H), 124.3 (21-CH), 118.9, 118.2 (2^1,3^1-CH), 101.2, 99.8 (5,20-CH), 98.1, 95.4 (10,15-CH), 33.0, 32.2, 32.00, 31.99, 31.94, 31.8, 29.9, 29.8, 26.8, 26.4 (12,13-CH_2), 22.93, 22.85, 20.11, 19.9 (8,17-CH_2), 18.4 (12,13-CH_2CH_3), 14.36, 14.28 (2 × $CH_2CH_2CH_3$), 12.02, 11.98 (8,17-CH_3). HRMS (ESI-TOF) m/z: $[M + H]^+$ calcd for $C_{52}H_{60}N_3^+$ 726.4782; Found 726.4789.

12,13-Diethyl-8,17-dihexyl-7,18,22-trimethylanthro[[2,3-*b*]carbaporphyrinato]palladium(II) (21). Palladium(II) acetate (7.5 mg, 0.045 mmol) was added to a solution of *N*-methylanthrocarbaporphyrin **111** (8.0 mg, 0.011 mmol) in a 1:1 mixture of acetonitrile-chloroform (8 mL), and the solution was stirred for 10 min at room temperature. The solvent was removed under reduced pressure, and the residue was purified on a silica column eluting with 2:3 dichloromethane-hexanes. The product was collected as a dark green fraction.

https://doi.org/10.1021/acs.joc.3c01839
J. Org. Chem. XXXX, XXX, XXX−XXX

Evaporation of the solvent and recrystallization of the residue from chloroform−methanol afforded the palladium complex (6.8 mg, 0.0082 mmol, 74%) as dark green crystals. UV−vis ($CHCl_3$; 1.1.332 × 10^{-5} M): λ_{max} (log ε) 331 (4.50), 436 (sh, 4.54), 477 (4.87), 496 (sh, 4.34), 609 (4.33), 627 (4.13), 688 (3.92). ^{1}H NMR (500 MHz, $CDCl_3$): δ 10.18 (s, 1H), 10.06 (s, 1H) (5,20-H), 9.71 (s, 1H), 9.61 (s, 1H) (10,15-H), 8.95 (s, 1H), 8.92 (s, 1H), (2^1,3^1-H), 8.62 (s, 2H, 2^2,3^2-H), 8.09−8.05 (m, 2H, 2^3,3^3-H), 7.50−7.46 (m, 2H, 2^4,3^4-H), 3.94−3.77 (m, 8H, 8,12,13,17-CH_2), 3.473 (s, 3H), 3.468 (s, 3H) (7,18-CH_3), 2.22 (p, 2H, J = 7.5 Hz), 2.09−1.97 (m, 2H) (8,17-CH_2CH_2), 1.85 (t, 3H, J = 7.7 Hz), 1.84 (t, 3H, J = 7.7 Hz) (12,13-CH_2CH_3), 1.77 (m, 2H), 1.66−1.59 (m, 2H), 1.58−1.48 (m, 2H), 1.47−1.31 (m, 6H), 0.94 (t, 3H, J = 7.3 Hz), 0.91 (t, 3H, J = 7.3 Hz) (2 × $CH_2CH_2CH_3$), −2.54 (s, 3H, N−CH_3). ^{13}C{^{1}H} NMR (125 MHz, $CDCl_3$): δ 151.5, 149.8, 147.5, 145.0, 143.9, 142.8, 142.5, 142.0, 140.8, 140.6, 140.4, 139.6, 138.0, 137.8, 135.8, 134.1, 133.1, 132.9, 132.4, 132.2, 131.7, 128.48, 128.41 (2^3,3^3-CH),127.2, 127.1 (2^2,3^2-CH), 125.3, 125.2 (2^4,3^4-CH), 116.5, 116.1 (2^1,3^1-CH), 107.2, 105.1 (5,20-CH), 101.2, 98.2 (10,15-CH), 48.5 (N−CH_3), 33.3, 32.2, 31.9, 31.3, 29.87, 29.85, 27.2, 26.8, 22.9, 22.8, 19.77, 19.75, 18.4, 18.2 (12,13-CH_2CH_3), 14,4, 14.2 (2 × $CH_2CH_2CH_3$), 12.4, 11.9 (7,18-CH_3). HRMS (ESI-TOF) m/z: M^+ calcd for $C_{52}H_{57}N_3Pd$ 829.3587; Found 829.3607.

12,13-Diethyl-8,17-dihexyl-7,18,21-trimethylanthro[[2,3-*b*]-carbaporphyrinato]palladium(II) (22). Palladium(II) acetate (10.1 mg, 0.045 mmol) was added to a solution of *N*-methylanthrocarbaporphyrin **20** (10.0 mg, 0.014 mmol) in a 1:1 mixture of acetonitrile-chloroform (8 mL), and the solution was stirred under reflux for 4 h. The solution was cooled, diluted with chloroform, and washed with water, and the organic layer was separated and then evaporated to dryness. The residue was chromatographed on silica, eluting with 30% dichloromethane-hexanes, and the product was collected as a reddish/brown band. The solvent was evaporated to dryness, and the residue was recrystallized from chloroform−methanol to yield the palladium-(II) complex (7.3 mg, 0.0088 mmol, 64%) as dark purple crystals, 188−190 °C. UV−vis ($CHCl_3$; 1.286 × 10^{-5} M): λ_{max}/nm (log ε) 348 (4.69), 449 (4.81), 762 (3.84), 841 (4.22). ^{1}H NMR (500 MHz, $CDCl_3$): δ 9.70 (s, 2H, 2^1,3^1-H), 9.55 (s, 2H, 5,20-H), 9.11 (s, 2H, 2^2,3^2-H), 8.84 (s, 2H, 10,15-H), 8.29−8.26 (m, 2H, 2^3,3^3-H), 7.63−7.60 (m, 2H, 2^4,3^4-H), 3.47−3.41 (m, 8H, 12,13−CH_2 and 8,17-CH_2CH_2), 3.05 (s, 6H, 7,18-CH_3), 2.23 (p, 4H, J = 7.5 Hz), 1.68−1.63 (m, 4H), 1.63 (t, 6H, J = 7.6 Hz, 12,13-CH_2CH_3), 1.51−1.45 (m, 4H), 1.44−1.37 (m, 4H), 0.94 (t, 6H, J = 7.3 Hz, 2 × $CH_2CH_2CH_3$), −1.45 (3H, s, 21-CH_3). ^{13}C{^{1}H} NMR (125 MHz, $CDCl_3$): δ 165.0, 153.3, 145.3, 142.1, 141.0, 139.9, 138.0, 132.5, 131.9, 131.3, 128.6 (2^3,3^3-CH), 127.4 (2^2,3^2-CH), 125.7 (2^4,3^4-CH), 120.6 (2^1,3^1-CH), 109.9 (10,15-CH), 107.3 (5,20-CH), 32.8, 32.1, 29.8, 26.42, 26.36, 22.9, 19.2, 18.1, 14.3 ($CH_2CH_2CH_3$), 11.5 (7,18-CH_3). HRMS (ESI-TOF) m/z: M^+ calcd for $C_{52}H_{57}N_3Pd$ 829.3587; Found 829.3599.

12,13-Diethyl-8,17-dihexyl-7,18,21-trimethylanthro[[2,3-*b*]-carbaporphyrinato](dicarbonyl)-rhodium(I) (18). Anhydrous sodium acetate (34.9 mg, 0.425 mmol, 10 equiv) and $[Rh(CO)_2Cl]_2$ (14.3 mg, 0.0368 mmol, 1 equiv) were added to a solution of anthro[2,3-*b*]carbaporphyrin **103** (25.3 mg, 0.0355 mmol, 1 equiv) in dichloromethane (24 mL), and the resulting mixture was refluxed with stirring under nitrogen overnight. The solvent was removed under reduced pressure, and the residue was purified by column chromatography on silica column eluting with 20% dichloromethane-hexanes. A broad green band was collected, the solvent evaporated, and the residue was recrystallized from chloroform/methanol to give **116** (11.5 mg, 0.0132 mmol, 37%) as dark green crystals, mp > 300 °C. UV−vis ($CHCl_3$; 1.170 × 10^{-5} M): λ_{max}/nm (log ε) 362 (4.02), 390 (sh, 4.64), 464 (sh, 4.55), 493 (4.97), 574 (4.10), 614 (4.32), 637 (sh, 4.02), 688 (3.39). ^{1}H NMR (500 MHz, $CDCl_3$): δ 10.30 (s, 1H), 10.07 (s, 1H) (5,20-H), 9.82 (s, 1H), 9.75 (s, 1H) (10,15-H), 9.28 (s, 1H), 9.22 (s, 1H) (2^1,3^1-H), 8.80 (s, 1H), 8.79 (s, 1H) (2^2,3^2-H), 8.16−8.13 (m, 2H, 2^3,3^3-H), 7.54−7.51 (m, 2H, 2^4,3^4-H), 4.11−3.84 (m, 7H), 3.82−3.75 (m, 1H) (6,12,13,17-CH_2), 3.66 (s, 3H), 3.53 (s, 3H) (7,18-CH_3), 2.33−2.24 (m, 2H), 2.15−2.06 (m, 2H), 1.84−1.80 (2 overlapping triplets, 6H, 12,13-CH_2CH_3), 1.77−1.71 (m, 2H), 1.70−1.63 (m, 2H), 1.55−1.45 (m, 4H), 1.42−1.34 (m, 4H), 0.92 (t, 6H, J = 7.3 Hz, 2 × $CH_2CH_2CH_3$), −2.36 (br s, 1H, NH), −4.91 (s, 1H, 21-H). ^{13}C{^{1}H} NMR (125 MHz, $CDCl_3$): 178.6 (d, $^1J_{Rh-C}$ = 67.0 Hz), 177.8 (d, $^1J_{Rh-C}$ = 68.6 Hz), 155.6, 153.6, 147.6, 146.7, 143.4, 142.6, 140.7, 139.5, 138.01, 137.93, 136.77, 136.65, 135.3, 133.1, 133.0, 132.59, 132.54, 132.31, 132.22, 132.20, 128.6 (2^3,3^3-CH), 127.4, 127.1 (2^2,3^2-CH), 125.45, 125.40 (2^4,3^4-CH), 125.34 (21-CH), 119.1, 118.8 (2^1,3^1-CH), 104.1, 103.4, 96.7, 94.3 (4 × *meso*-CH), 33.0, 32.8 (8,17-CH_2CH_2), 32.19, 32.13 (2 × $CH_2CH_2CH_3$), 30.0, 29.9 (8,17-$CH_2CH_2CH_2$), 26.8, 26.6 (8,17-CH_2), 22.9 (12,13-CH_2), 20.6, 20.0 (2 × $CH_2CH_2CH_3$), 18.2, 18.1 (12,13-CH_2CH_3), 14.24, 14.23 (2 × $CH_2CH_2CH_3$), 12.5, 11.7 (7,18-CH_3). HRMS (ESI-TOF) m/z: M^+ calcd for $C_{53}H_{56}N_3O_2Rh$ 869.3428; Found 869.3448.

Computational Studies. All calculations were performed using the Gaussian 16 revision C.01.35 Geometry optimizations were performed using the M06-2X functional and the 6-311++G(d,p) basis set.[36] Palladium complexes were modeled using the Los Alamos LANL2DZ basis.[37] Vibrational frequencies were computed to confirm the absence of imaginary frequencies and derive zero-point energy and vibrational entropy corrections from unscaled frequencies. Single point energy calculations were performed on the optimized minima using M06-2X/cc-PVTZ.[38] NICS values were calculated using the GIAO method,[39] and AICD plots were obtained from CGST calculations.[40] NICS(0) was calculated at the mean position of all four heavy atoms in the middle of the macrocycle. NICS(a), NICS(b), NICS(c), NICS(d), NICS(e), NICS(f), and NICS(g) values were obtained by applying the same method to the mean position of the heavy atoms that comprise the individual rings of each macrocycle. In addition, $NICS(1)_{zz}$, $NICS(1a)_{zz}$, $NICS(1b)_{zz}$, $NICS(1c)_{zz}$, $NICS(1d)_{zz}$, $NICS(1e)_{zz}$, $NICS(1f)_{zz}$, and $NICS(1g)_{zz}$ were obtained by applying the same method to ghost atoms placed 1 Å above each of the corresponding NICS(0) points and extracting the zz contribution of the magnetic tensor. The resulting energies, Cartesian coordinates, and AICD plots can be found in the Supporting Information.

■ ASSOCIATED CONTENT

Data Availability Statement

The data underlying this study are available in the published article and its online Supporting Information.

Supporting Information

The Supporting Information is available free of charge at https://pubs.acs.org/doi/10.1021/acs.joc.3c01839.

Tables giving Cartesian coordinates; calculated energies; selected bond lengths and AICD plots; and selected UV−vis, ^{1}H NMR, ^{1}H−^{1}H COSY, HSQC, DEPT-135, ^{13}C{^{1}H} NMR, and mass spectra (PDF)

■ AUTHOR INFORMATION

Corresponding Author

Timothy D. Lash − *Department of Chemistry, Illinois State University, Normal, Illinois 61790-4160, United States;* orcid.org/0000-0002-0050-0385; Email: tdlash@ilstu.edu

Authors

Melissa A. Mathius − *Department of Chemistry, Illinois State University, Normal, Illinois 61790-4160, United States*

Justin M. Chhoeun − *Department of Chemistry, Illinois State University, Normal, Illinois 61790-4160, United States*

Riley H. Kaufman − *Department of Chemistry, Illinois State University, Normal, Illinois 61790-4160, United States*

Deyaa I. AbuSalim − *Department of Chemistry, Illinois State University, Normal, Illinois 61790-4160, United States*

Complete contact information is available at: https://pubs.acs.org/10.1021/acs.joc.3c01839

https://doi.org/10.1021/acs.joc.3c01839
J. Org. Chem. XXXX, XXX, XXX−XXX

Notes

The authors declare no competing financial interest.

■ ACKNOWLEDGMENTS

This work was supported by the National Science Foundation under grants CHE-1855240 and CHE-2247214. NSF is also acknowledged for providing funding for the departmental NMR spectrometers (CHE-0722385) and mass spectrometer (CHE-1337497) under the Major Research Instrumentation (MRI) program.

■ REFERENCES

(1) Lash, T. D. Carbaporphyrinoid Systems. *Chem. Rev.* **2017**, *117*, 2313−2446.

(2) Lash, T. D. Organometallic Chemistry within the Structured Environment Provided by the Macrocyclic Cores of Carbaporphyrins and Related Systems. *Molecules* **2023**, *28*, 1496.

(3) (a) Thuita, D. W.; Brückner, C. Metals Complexes of Porphyrinoids Containing Nonpyrrolic Heterocycles. *Chem. Rev.* **2022**, *122*, 7990−8052. (b) Toganoh, M.; Furuta, H. Creation from Confusion to Fusion in the Porphyrin World-The Last Three Decades of *N*-Confused Porphyrinoid Chemistry. *Chem. Rev.* **2022**, *122*, 8313−8437. (c) Białek, M. J.; Hurej, K.; Furuta, H.; Latos-Grażyński, L. Organometallic Chemistry Confined within a Porphyrin-like Framework. *Chem. Soc. Rev.* **2023**, *52*, 2082−2144.

(4) Lash, T. D.; Hayes, M. J. Carbaporphyrins. *Angew. Chem., Int. Ed.* **1997**, *36*, 840−842.

(5) Lash, T. D.; Colby, D. A.; Szczepura, L. F. New Riches in Carbaporphyrin Chemistry: Silver and Gold Organometallic Complexes of Benzocarbaporphyrins. *Inorg. Chem.* **2004**, *43*, 5258−5267.

(6) Adiraju, V. A. K.; Ferrence, G. M.; Lash, T. D. Rhodium(I), Rhodium(III) and Iridium(III) Carbaporphyrins. *Dalton Trans.* **2016**, *45* (35), 13691−13694.

(7) Alemayehu, A. B.; Vasquez-Lima, H.; Teat, S. J.; Ghosh, A. Unexpected Molecular Structure of a Putative Rhenium-Dioxo-Benzocarbaporphyrin Complex. Implications for the Highest Transition Metal Valence in a Porphyrin-Type Ligand Environment. *ChemistryOpen* **2019**, *8*, 1298−1302.

(8) Lash, T. D.; Muckey, M. A.; Hayes, M. J.; Liu, D.; Spence, J. D.; Ferrence, G. M. Regioselective Oxidation of Benzocarbaporphyrins with Ferric Chloride: A Facile Synthesis of Bridged [18]Annulene Ketals with Strong Absorptions in the Far Red and an Unexpected Halogenation Reaction at the Interior Carbon Atom. *J. Org. Chem.* **2003**, *68*, 8558−8570.

(9) Taylor, V. M.; Cedeño, D. L.; Muñoz, D. L.; Jones, M. A.; Lash, T. D.; Young, A. M.; Constantino, M. H.; Esposito, N.; Vélez, I. D.; Robledo, S. M. *In Vivo* and *In Vitro* Studies of the Utility of Dimethyl and Diethyl Carbaporphyrin Ketals in the Treatment of Cutaneous Leishmaniasis. *Antimicrob. Agents Chemother.* **2011**, *55*, 4755−4764, DOI: 10.1128/AAC.00671-11.

(10) Lash, T. D. Unexpected alkyl group migration in palladium(II) benzocarbaporphyrins. *Org. Lett.* **2011**, *13*, 4632−4635.

(11) Latham, A. N.; Ferrence, G. M.; Lash, T. D. Metalation and Methyl Group Migration in 21-, 22- and 23-Methylcarbaporphyrins: Synthesis and Characterization of Palladium(II), Rhodium(I) and Rhodium(III) Derivatives. *Organometallics* **2019**, *38*, 575−585.

(12) (a) Allard, S.; Forster, M.; Souharce, B.; Thiem, H.; Scherf, U. Organic Semiconductors for Solution-Processable Field-Effect Transistors (OFETs). *Angew. Chem., Int. Ed.* **2008**, *47*, 4070−4098. (b) Wang, C.; Dong, H.; Hu, W.; Liu, Y.; Zhu, D. Semiconducting π-Conjugated Systems in Field-Effect Transistors: a Material Odyssey of Organic Electronics. *Chem. Rev.* **2012**, *112*, 2208−2267.

(13) Panwar, N.; Soehartono, A. M.; Chan, K. K.; Zeng, S.; Xu, G.; Qu, J.; Coquet, P.; Yong, K.-T.; Chen, X. Nanocarbons for Biology and Medicine: Sensing, Imaging, and Drug Delivery. *Chem. Rev.* **2019**, *119*, 9559−9656.

(14) (a) Yang, G.; Liu, L.; Yang, Q.; Wang, S. Tetraacenaphthoporphyrin: A π-Conjugated Porphyrin with Efficient Light-Activated Anticancer Activity. *Chem. − Asian J.* **2011**, *6*, 1147−1150. (b) Gardner, D. M.; Taylor, V. M.; Cedeño, D. L.; Padhee, S.; Robledo, S. M.; Jones, M. A.; Lash, T. D.; Vélez, I. D. Association of Acenaphthoporphyrins with Liposomes for the Photodynamic Treatment of Leishmaniasis. *Photochem. Photobiol.* **2010**, *86*, 645−652.

(15) (a) Stępień, M.; Gonka, E.; Zyła, M.; Sprutta, N. Heterocyclic Nanographenes and Other Polycyclic Heteroaromatic Compounds: Synthetic Routes, Properties and Applications. *Chem. Rev.* **2017**, *117*, 3479−3716. (b) Borissov, A.; Maurya, M. K.; Moshniaha, L.; Wong, W.-S.; Zyla-Karwowska, M.; Stępień, M. Recent Advances in Heterocyclic Nanographenes and Other Polycyclic Heteroaromatic Compounds. *Chem. Rev.* **2022**, *122*, 565−788.

(16) Wang, X.-Y.; Yao, X.; Narita, A.; Müllen, K. Heteroatom-Doped Nanographenes with Structural Precision. *Acc. Chem. Res.* **2019**, *52*, 2491−2505.

(17) Grabowski, E. Y.; AbuSalim, D. I.; Lash, T. D. Naphtho[2,3-*b*]carbaporphyrins. *J. Org. Chem.* **2018**, *83*, 11825−11838.

(18) For examples of anthroporphyrins, see: (a) Kobayashi, N.; Nevin, W. A.; Mizunuma, S.; Awaji, H.; Yamaguchi, M. Ring-expanded Porphyrins as an Approach Towards Highly Conductive Molecular Semiconductors. *Chem. Phys. Lett.* **1993**, *205*, 51−54. (b) Yamada, H.; Kuzuhara, D.; Takahashi, T.; Shirnizu, Y.; Uota, K.; Okujima, T.; Uno, H.; Ono, N. Synthesis and Characterization of Tetraanthroporphyrins. *Org. Lett.* **2008**, *10*, 2947−2950. (c) Filatov, M. A.; Baluschev, S.; Ilieva, I. Z.; Enkelmann, V.; Miteva, T.; Landfester, K.; Aleshchenkov, S. E.; Cheprakov, A. V. Tetraaryltetraanthra[2,3]porphyrins: Synthesis, Structure, and Optical Properties. *J. Org. Chem.* **2012**, *77*, 11119−11131.

(19) Patney, H. K.; Paddon-Row, M. N. An Improved Synthesis of 2,3-Norbornadienoanthracene and Its Application to the Synthesis of Anthracene Annellated Norbornenylogs. *Synthesis* **1986**, *1986*, 326−328.

(20) Lash, T. D. What's in a Name? The MacDonald Condensation. *J. Porphyrins Phthalocyanines* **2016**, *20*, 855−888, DOI: 10.1142/S1088424616300147.

(21) Lash, T. D.; Mathius, M. A.; AbuSalim, D. I. Synthesis of Chrysoporphyrins and a Related Benzopyrene-fused System. *J. Org. Chem.* **2022**, *87*, 16276−16296.

(22) Mironov, A.; Kadish, K. M.; Smith, K. M.; Guilard, R. *Handbook of Porphyrin Science-With Applications to Chemistry, Physics, Material Science, Engineering, Biology and Medicine*; World Scientific Publishing: Singapore, 2012; Vol. *18*, pp 303−413.

(23) Lash, T. D.; Darrow, W. T.; Latham, A. N.; Sahota, N.; Ferrence, G. M. Rhodium Complexes of Carbaporphyrins, Carbachlorins, *adj*-Dicarbaporphyrins and an *adj*-Dicarbachlorin. *Inorg. Chem.* **2019**, *58*, 7511−7526.

(24) Latham, A. N.; Lash, T. D. Synthesis and Characterization of *N*-Methylporphyrins, Heteroporphyrins, Carbaporphyrins and Related Systems. *J. Org. Chem.* **2020**, *85*, 13050−13068.

(25) Li, D.; Lash, T. D. Synthesis and Reactivity of Carbachlorins and Carbaporphyrins. *J. Org. Chem.* **2014**, *79*, 7112−7121.

(26) Wu, J. I.; Fernandez, I.; Schleyer, P. v. R. Description of Aromaticity in Porphyrinoids. *J. Am. Chem. Soc.* **2013**, *135*, 315−321.

(27) Ghosh, A. First-Principles Quantum Chemical Studies of Porphyrins. *Acc. Chem. Res.* **1998**, *31*, 189−198.

(28) Aihara, J.-i.; Nakagami, Y.; Sekine, R.; Makino, M. Validity and Limitations of the Bridged Annulene Model for Porphyrins. *J. Phys. Chem. A* **2012**, *116*, 11718−11730.

(29) Valiev, R. R.; Fleigl, H.; Sundholm, D. Predicting the Degree of Aromaticity of Novel Carbaporphyrinoids. *Phys. Chem. Chem. Phys.* **2015**, *17*, 14215−14222.

(30) AbuSalim, D. I.; Lash, T. D. Aromatic Character and Relative Stability of Pyrazoloporphyrin Tautomers and Related Protonated Species: Insights into How Pyrazole Changes the Properties of Carbaporphyrinoid Systems. *Molecules* **2023**, *28*, 2854.

(31) AbuSalim, D. I.; Lash, T. D. Relative Stability and Diatropic Character of Carbaporphyrin, Dicarbaporphyrin, Tricarbaporphyrin and Quatyrin Tautomers. *J. Org. Chem.* **2013**, *78*, 11535−11548.

https://doi.org/10.1021/acs.joc.3c01839
J. Org. Chem. XXXX, XXX, XXX−XXX

(32) AbuSalim, D. I.; Lash, T. D. Aromatic Character and Stability of Neo-Confused Porphyrin Tautomers and Related Compounds. *Org. Biomol. Chem.* **2013**, *11*, 8306−8323.
(33) Schleyer, P. v. R.; Maerker, C.; Dransfeld, A.; Jiao, H.; van Eikema Hommes, N. J. R. Nucleus-Independent Chemical Shifts: a Simple and Efficient Aromaticity Probe. *J. Am. Chem. Soc.* **1996**, *118*, 6317−6318.
(34) Geuenich, D.; Hess, K.; Köhler, F.; Herges, R. Anisotropy of Induced Current Density (ACID), a General Method to Quantify and Visualize Electronic Delocalization. *Chem. Rev.* **2005**, *105*, 3758−3772.
(35) Frisch, M. J.; Trucks, G. W.; Schlegel, H. B.; Scuseria, G. E.; Robb, M. A.; Cheeseman, J. R.; Scalmani, G.; Barone, V.; Petersson, G. A.; Nakatsuji, H.; Li, X.; Caricato, M.; Marenich, A. V.; Bloino, J.; Janesko, B. G.; Gomperts, R.; Mennucci, B.; Hratchian, H. P.; Ortiz, J. V.; Izmaylov, A. F.; Sonnenberg, J. L.; Williams-Young, D.; Ding, F.; Lipparini, F.; Egidi, F.; Goings, J.; Peng, B.; Petrone, A.; Henderson, T.; Ranasinghe, D.; Zakrzewski, V. G.; Gao, J.; Rega, N.; Zheng, G.; Liang, W.; Hada, M.; Ehara, M.; Toyota, K.; Fukuda, R.; Hasegawa, J.; Ishida, M.; Nakajima, T.; Honda, Y.; Kitao, O.; Nakai, H.; Vreven, T.; Throssell, K.; Montgomery, J. A., Jr; Peralta, J. E.; Ogliaro, F.; Bearpark, M. J.; Heyd, J. J.; Brothers, E. N.; Kudin, K. N.; Staroverov, V. N.; Keith, T. A.; Kobayashi, R.; Normand, J.; Raghavachari, K.; Rendell, A. P.; Burant, J. C.; Iyengar, S. S.; Tomasi, J.; Cossi, M.; Millam, J. M.; Klene, M.; Adamo, C.; Cammi, R.; Ochterski, J. W.; Martin, R. L.; Morokuma, K.; Farkas, O.; Foresman, J. B.; Fox, D. J. *Gaussian 16*, Revision C.01; Gaussian, Inc.: Wallingford, CT, 2019.
(36) (a) Clark, T.; Chandrasekhar, J.; Spitznagel, G. W.; Schleyer, R. v. P. Efficient Diffuse Function-augmented Basis Sets for Anion Calculations. III. The 3-21+G Basis Set for First-Row Elements, Li-F. *J. Comput. Chem.* **1983**, *4*, 294−301. (b) Ditchfield, R.; Hehre, W. J.; Pople, J. A. Self-Consistent Molecular-Orbital Methods. IX. An Extended Gaussian-Type Basis for Molecular-Orbital Studies of Organic Molecules. *J. Chem. Phys.* **1971**, *54*, 724−728. (c) Hariharan, P. C.; Pople, J. A. The Influence of Polarization Functions on Molecular Orbital Hydrogenation Energies. *Theor. Chim. Acta* **1973**, *28*, 213−222. (d) Hehre, W. J.; Ditchfield, R.; Pople, J. A. Self-Consistent Molecular Orbital Methods. XII. Further Extensions of Gaussian-Type Basis Sets for Use in Molecular Orbital Studies of Organic Molecules. *J. Chem. Phys.* **1972**, *56*, 2257−2261.
(37) Wadt, W. R.; Hay, J. *Ab Initio* Effective Core Potentials for Molecular Calculations. Potentials for Main Group Elements Na to Bi. *J. Chem. Phys.* **1985**, *82*, 284−298.
(38) Dunning, T. H., Jr. Gaussian Basis Sets for use in Correlated Molecular Calculations. I. The Atoms Boron through Neon and Hydrogen. *J. Chem. Phys.* **1989**, *90*, 1007−1023.
(39) Chen, Z.; Wannere, C. S.; Corminboeuf, C.; Puchta, R.; Schleyer, P. v. R. Nucleus-Independent Chemical Shifts (NICS) as an Aromaticity Criterion. *Chem. Rev.* **2005**, *105*, 3842−3888.
(40) Herges, R.; Geuenich, D. Delocalization of Electrons in Molecules. *J. Phys. Chem. A* **2001**, *105*, 3214−3220.

https://doi.org/10.1021/acs.joc.3c01839
J. Org. Chem. XXXX, XXX, XXX−XXX